Anchoring and Synaptic stability of PSD-95 is driven by ephrin-B3

Martin Hruska, **Nathan T. Henderson**, **Nan L. Xia**, **Sylvain J. Le Marchand**[1], and **Matthew B. Dalva**[*]

Department of Neuroscience and the Farber Institute for Neuroscience, Thomas Jefferson University, Jefferson Hospital for Neuroscience, 900 Walnut Street, Philadelphia, PA 19107, USA

Summary

Organization of signaling complexes at excitatory synapses by Membrane Associated Guanylate Kinase (MAGUK) proteins regulates synapse development, plasticity, senescence, and disease. Post-translational modification of MAGUK family proteins can drive their membrane localization, yet it is unclear how these intracellular proteins are targeted to sites of synaptic contact. Here we show using super-resolution imaging, biochemical approaches, and *in vivo* models that the *trans*-synaptic organizing protein, ephrin-B3, controls the synaptic localization and stability of PSD-95 and links these events to changes in neuronal activity via negative regulation of a novel MAPK-dependent phosphorylation site on ephrin-B3 (S332). Unphosphorylated ephrin-B3 is enriched at synapses, interacts directly with and stabilizes PSD-95 at synapses. Activity induced phosphorylation of S332 disperses ephrin-B3 from synapses, prevents the interaction with, and enhances the turnover of PSD-95. Thus, ephrin-B3 specifies the synaptic localization of PSD-95 and likely links the synaptic stability of PSD-95 to changes in neuronal activity.

Introduction

Synaptic function requires the dynamic regulation of proteins within the postsynaptic density (PSD). MAGUK scaffold proteins such as PSD-95 cluster within the PSD and interact with synaptic proteins to organize and regulate the synaptic signaling complex [1]. PSD-95 regulates the trafficking and localization of proteins such as AMPA and NMDA-type glutamate receptors and synaptic signaling molecules to modulate plasticity by linking

[*]**Contact information for corresponding author:** Matthew B. Dalva, Associate Professor, Department of Neuroscience and the Farber Institute for Neuroscience, Thomas Jefferson University, Jefferson Hospital for Neuroscience, suite 463, 900 Walnut Street, Philadelphia, PA 19107, USA, Tel: 215-503-1007 (lab), 215-503-0997 (Office), Matthew.Dalva@jefferson.edu.
[1]Current Address: Cell Imaging Center, Papadakis Integrated Sciences Building B401.N2, Drexel University, Philadelphia, PA, sjl99@drexel.edu, Phone: (215) 571-4053
Martin.Hruska@jefferson.edu
nathan.henderson@jefferson.edu
Nan.Xia@jefferson.edu

changes in neuronal activity to changes in gene expression [2]. During development increases or decreases in PSD-95 expression levels result in formation of higher or lower numbers of excitatory synapses, respectively [3-5]. Moreover, defects in MAGUK function are linked to cognitive, social, and motoric phenotypes found in mouse models and human disease such as Schizophrenia and Intellectual Disability [6,7]. However, despite the importance of PSD-95 at excitatory synapses, little is known about how PSD-95 is organized, recruited, and stabilized at synaptic sites.

To control the organization, development and function of excitatory synapses, PSD-95 must be maintained within the PSD, yet 20-40% of synaptic PSD-95 turns over every 20-30 minutes [8-11]. The turnover of PSD-95 is regulated by activity-dependent phosphorylation, PDZ domain driven protein-protein interactions, and post-translational modification of PSD-95 [11-15]. Palmitoylation of PSD-95 within the PSD enhances the membrane localization and retention of PSD-95, but is not sufficient for the accumulation of PSD-95 at synapses [16].

How might PSD-95 become stabilized at or targeted to synaptic sites? One attractive hypothesis is that PSD-95 could interact with synapse adhesion molecules that initiate synapse formation and maturation [17]. Although several classes of trans-synaptic molecules can interact with PSD-95, none are known to direct PSD-95 to synapses [18-20]. Thus, a molecule directing the localization of PSD-95 to synapses has yet to be identified.

The ephrin-B family of molecules (ephrin-B1-3) can act as synaptic adhesion and signaling proteins and are linked to both pre and postsynaptic development and function [21]. Ephrin-Bs signal to a number of proteins and bind to and activate Eph receptor tyrosine kinases [21]. One ephrin-B in particular, ephrin-B3, functions postsynaptically to control the density of excitatory synapses through a competitive mechanism that negatively regulates the MAPK pathway by a direct interaction with ERK kinase [22]. Importantly, similar to PSD-95, the level of ephrin-B3 expression within a neuron controls the density of synapses such that neurons with higher levels of ephrin-B3 have a competitive advantage and receive more synapses than neurons expressing less ephrin-B3 [22]. However, whether PSD-95 and ephrin-B3 function in the same pathway is unknown.

Here, using a combination of high-resolution imaging, biochemistry, and fluorescence recovery after photobleaching (FRAP), we show that ephrin-B3 controls the synaptic localization and turnover of PSD-95 by interacting directly with PSD-95 at synapses *in vitro* and *in vivo*. Importantly, ephrin-B3 dependent regulation of PSD-95 is modulated by neuronal activity and sensory deprivation through a negative regulatory mechanism that relies on the phosphorylation of ephrin-B3 at S332 by MAPK kinase signaling. Thus, we provide the first example of a *trans*-synaptic signal that controls the synaptic localization of PSD-95.

Results

Ephrin-B3 and PSD-95 interact at synapses

Both PSD-95 and ephrin-B3 are found at synapses and the overexpression or knockdown of either molecule results in similar synaptic phenotypes [3,5,22], suggesting that they might be found in the same biochemical complex.

To test whether ephrin-B3 and PSD-95 co-localize at synapses within the same dendritic spine, we conducted two-color super resolution imaging using stimulated emission depletion (STED; ~80 nm resolution; Leica SP5 CW STED confocal) microscopy of tdTomato transfected DIV20-22 cortical neurons [23]. Four-color images with two-color STED (endogenous PSD-95 (Neuromab) and ephrin-B3 (Invitrogen)) and two-color conventional confocal (endogenous vGlut1 (Milipore) and tdTomato) were collected to visualize the localization of these proteins in single spines (Fig. 1a). Consistent with the location of the epitopes of the antibodies to PSD-95 and ephrin-B3 (Methods) and the reported organization of PSD-95 and ephrin-B3 [21,24,25], STED imaging resolved discrete puncta of both PSD-95 and ephrin-B3 within many spines. The majority of vGlut1$^+$ spines (~80% of 248 spines) had clusters of both ephrin-B3 and PSD-95 (Fig.1b-c; 162 spines out of 202 vGlut$^+$ spines). In contrast, at vGlut1$^+$ dendritic spines, puncta of either PSD-95 or ephrin-B3 were rarely found alone (Fig.1c). These results suggest that ephrin-B3 and PSD-95 co-localize at sites of synaptic contact within dendritic spines.

Next, we sought to determine whether ephrin-B3 and PSD-95 are found in the same biochemical complex *in vivo*. Whole brain lysates (Fig. 1d-f, Supplementary Fig. 1a) and purified synaptosomes were made (Fig. 1g-i, Supplementary Fig. 1b) from P21 wild type and ephrin-B3 null (*Efnb3$^{-/-}$*) mouse brains. We then immunoprecipitated ephrin-B3 using an ephrin-B3 antibody and asked whether PSD-95 co-immunoprecipitated (co-IP-ed) with ephrin-B3. Ephrin-B3 IP-ed from both whole brain lysates and synaptosomes of wild type animals (Fig. 1e, h), and appeared as a doublet, likely due to post-translational modification [26]. These bands were absent in lysates and IP samples from *Efnb3$^{-/-}$* animals indicating antibody specificity (Fig. 1e, h). Consistent with the idea that ephrin-B3 and PSD-95 interact only at synaptic sites, PSD-95 co-IP-ed with ephrin-B3 only from synaptosomes isolated from brains of wild type animals (Fig. 1g, Supplementary Fig. 1b) and we failed to detect the co-IP of PSD-95 in whole brain lysates or from *Efnb3$^{-/-}$* mice (Fig.1d, Supplementary Fig. 1a). These data indicate that ephrin-B3 and PSD-95 are found in the same biochemical complex selectively at synapses *in vivo*.

To test whether ephrin-B3 and PSD-95 interaction at synapses is specific to ephrin-B3 or whether it is a general feature of the ephrin-B family of proteins, we immunoprecipitated each of the three ephrin-B family members from cortical synaptosomes and tested whether PSD-95 co-IP-ed (Fig. 1j-l, Supplementary Fig.1c). Despite their high sequence homology with ephrin-B3 (Fig. 2a), ephrin-B1 and ephrin-B2 did not co-IP PSD-95 from synaptosomes (Fig.1j). Similarly, in an *in vitro* binding assay, ephrin-B1 and ephrin-B2 bound PSD-95-GST much less well than ephrin-B3 (Supplementary Fig. 1d-f). These experiments demonstrate that the interaction with PSD-95 is specific to ephrin-B3, occurs at

synapses *in vivo* and *in vitro*, and suggest that regions of ephrin-B3 other than the highly conserved PDZ binding domain may be responsible for the PSD-95/ephrin-B3 interaction.

Distinct MAPK domains on ephrin-B3 regulate PSD-95 binding

Ephrin-B3 binds ERK2 through an ERK binding D-domain in its juxtamembrane region. This domain is unique to ephrin-B3 and enables ephrin-B3 to act as a negative regulator of MAPK signaling by inhibiting the nuclear translocation of ERK2 [22] (Fig 2a). In addition, we identified a putative MAPK phosphorylation consensus site at serine-332 (S332, PPQSPP) immediately upstream of the ephrin-B3 PDZ binding domain (Fig. 2a).

To test whether ERK signaling might regulate the ability of ephrin-B3 to interact with PSD-95, we used our previously characterized ephrin-B3 D-domain (L293A) mutant that disrupts the interaction with ERK2 and leads to more active ERK signaling [22], and ephrin-B3 mutants of S332 that either mimic phosphorylation (S332D) or render ephrin-B3 non-phosphorylatable (S332A). The wild type and mutant flag-tagged ephrin-B3 (flag-eB3) constructs were tested for their ability to co-IP PSD-95-GFP (Fig. 2b, Supplementary Fig. 2a, b). To account for differences in the expression of each flag-ephrin-B3 construct, the amount of PSD-95-GFP co-IP-ed was normalized to the amount of the flag-ephrin-B3 protein expressed in the lysates of that condition (Fig. 2c). Consistent with our findings *in vivo*, PSD-95-GFP co-IP-ed with wild type flag-eB3 when co-expressed in HEK293T cells (Fig 2b,c, Supplementary Fig. 2a, b). In contrast, the flag-eB3 D-domain mutant (L293A) exhibited significantly reduced co-immunoprecipitation of PSD-95-GFP compared to wild type flag-eB3 (Fig 2b,c, Supplementary Fig. 2a, b, p<0.01, ANOVA), indicating that the ERK-binding D-domain is important for ephrin-B3/PSD-95 interaction. Moreover, significantly less PSD-95-GFP co-IP-ed with the flag-eB3 mutant that mimics S332 phosphorylation (flag-eB3-S332D) than with wild type flag-eB3 (Fig. 2b, c,, Supplementary Fig. 2a, b, p<0.05, ANOVA). Mutation of S332 to a non-phosphorylatable alanine residue (flag-eB3-S332A) did not significantly alter the co-IP of PSD-95-GFP compared to wild type flag-eB3 (Fig. 2b, c;, Supplementary Fig. 2a, b, p = 0.8739, ANOVA). Thus, the mutations in ephrin-B3 that result in or that simulate increased ERK signaling also result in reduced association with PSD-95-GFP, suggesting that ERK signaling negatively regulates the ephrin-B3/PSD-95 interaction.

To further examine the nature of the ephrin-B3/PSD-95 interaction and the importance of the ephrin-B3 intracellular domain for its regulation, we performed *in vitro* binding experiments using a PSD-95-GST fusion protein and the cytosolic domains of ephrin-B3. Flag-tagged wild type and mutant ephrin-B3 cytosolic domain proteins were made by *in vitro* translation (Invitrogen), purified using flag antibody-coated beads, and then incubated with 160 ng of PSD-95-GST. Remarkably, both the wild type and S332A ephrin-B3 mutant intracellular domains pulled down PSD-95-GST (Figure 2d, e, Supplementary Fig. 2c). These constructs also depleted PSD-95-GST from the flow-through (not shown). In contrast, the S332D ephrin-B3 mutant failed to pull-down PSD-95-GST (Fig. 2d, e, Supplementary Fig. 2c, p<0.05, ANOVA). These findings indicate that the ephrin-B3 intracellular domain binds directly to PSD-95 and that this interaction requires S332.

S332 in ephrin-B3 controls the localization of PSD-95

To better understand the role of the S332 residue in ephrin-B3, we asked whether mutation of S332 might alter the synaptic localization of ephrin-B3 and PSD-95 using super resolution imaging and a molecular replacement strategy [22]. The impact of S332 on the synaptic localization of PSD-95 was analyzed in neurons rescued with shRNA-resistant wild type, phosphomimetic (S332D) or non-phosphorylatable (S332A) flag-eB3 constructs . Effects on synaptic localization of ephrin-B3 (flag) and endogenous PSD-95 were analyzed by STED imaging (~80nm resolution) at DIV21 when neurons have many dendritic spines and mature synapses [27] (Fig. 2 f). Synaptic sites were defined by the presence of vGlut1 staining (~ 250nm resolution, Fig. 2 f), and the expression level of flag-eB3 rescue constructs was the same for all conditions (Supplementary Fig. 2d-f). As expected from imaging of endogenous ephrin-B3 (Fig. 1), wild type flag-eB3 localized to dendritic spines (Fig. 2f (flag), g; >80% of 89 total spines) and was enriched in dendritic spines with both PSD-95 and vGlut1 (Fig. 2f (merge), h; 76% out of 65 vGlut1$^+$ spines).

Mutations to ephrin-B3 (flag-eB3-S332D rescue), which rendered it unable to interact with PSD-95, resulted in significantly reduced localization of both endogenous PSD-95 and flag-eB3-S332D to spines (Fig 2f (PSD-95, Flag), g; p<0.0001, ANOVA). Moreover, expression of flag-eB3-S332D resulted in a 50% reduction of ephrin-B3/PSD-95 co-clusters in vGlut1$^+$ spines (Fig. 2h; 41% out of 248 vGlut1$^+$ spines, p<0.0001, ANOVA). Although the number of synapses on flag-eB3-S332D transfected neurons was reduced (Fig. 2i and images in Supplementary Fig. 2d, e, p<0.0001, ANOVA), the proportion of spines associated with presynaptic terminals (vGlut1$^+$ spines) was similar to control (Fig 2g; 78% out of 318 total spines, p=0.91, ANOVA). These findings suggest that phosphorylation of S332 reduces the synaptic localization of both ephrin-B3 and PSD-95.

In contrast, the flag-eB3-S332A rescue mutant was enriched in dendritic spines and often found at synaptic sites (Fig. 2f). The proportion of spines containing flag-eB3-S332A and endogenous PSD-95 co-clusters was significantly higher than the proportion in neurons transfected with the non-PSD-95 binding flag-eB3-S332D phosphomimetic mutant (Fig. 2g,; >80% of 247 spines, p<0.0001, ANOVA). Interestingly, expression of flag-eB3-S332A led to a small but significant increase in the proportion of vGlut1$^+$ spines (Fig. 2g; 89% out of 247 total spines, p<0.05, ANOVA), suggesting that in neurons the unphosphorylated form of ephrin-B3 may act dominantly to recruit PSD-95 and ephrin-B3 to synaptic sites. Ephrin-B3 might then act in a transsynaptic fashion to induce presynaptic maturation [22]. Consistent with this, we observed significantly more co-localization of flag-eB3-S332A and PSD-95 in vGlut1$^+$ spines than in neurons transfected with flag-eB3-S332D (Fig. 2h; 78% out of 207 vGlut1$^+$ spines, p<0.0001, ANOVA). These results indicate that the synaptic localization of ephrin-B3 and PSD-95 and the PSD-95/ephrin-B3 interaction are likely mediated by ephrin-B3 that is not phosphorylated at S332.

The PSD-95 ephrin-B3 interaction regulates synapse density

Ephrin-B3 regulates synapse density in cortical neurons [22]. Given the role of PSD-95 in the maturation of excitatory synapses [3-5], we asked whether the ability of ephrin-B3 to interact with PSD-95 might regulate synapse density using a molecular replacement strategy. As

expected, mutations to ephrin-B3 that reduce the ability of ephrin-B3 to interact with PSD-95 (L293A and S332D) fail to rescue decreased synapse density resulting from ephrin-B3 knockdown, while mutations that promote this interaction (WT and S332A) rescue synapse density (Fig. 2i; see images in Supplementary Fig. 2d, e, p<0.0001, ANOVA). Interestingly, synapse density in flag-eB3-S332A expressing neurons was significantly higher than both control and wild type flag-eB3 rescue conditions (Fig. 2t and Supplementary Fig. 2e, p<0.05, ANOVA). These findings are consistent with the model where ephrin-B3 binding to ERK enhances both synapse density and ephrin-B3/PSD-95 binding, while the phosphorylation of S332 negatively regulates synapse density, likely by disrupting the interaction between ephrin-B3 and PSD-95 or their localization.

MAPKs phosphorylate ephrin-B3 in an activity dependent fashion

S332 of ephrin-B3 is necessary and sufficient for binding to PSD-95 and S332 resides within a putative MAPK phosphorylation motif PPQSPP. To determine whether ephrin-B3 might be phosphorylated by MAPK at S332, we raised a specific antibody directed against this site (pS332, Supplementary Fig. 3a-h, see Online Methods). Using the phospho-S332 specific antibody, we tested whether ephrin-B3 might undergo neuronal activity-dependent MAPK phosphorylation at S332 in cortical neurons [28] (Fig. 3a). DIV 14 cortical neurons were depolarized (55mM KCl) for one hour, which triggered activation of ERK1/2 and induced a significant 1.92 ± 0.17-fold increase above TTX-treated baseline in phospho S332 signal (Fig. 3b, c, p<0.001, ANOVA). The effects of depolarization were blocked by pre-treatment of neurons with MEK inhibitors (U0126, 10 μM, Sigma, Fig. 3b, c, Supplementary Fig. 4a or PD98059, 100 μM, Sigma, Supplementary Fig. 4b-d,), suggesting that S332 is phosphorylated by ERK/MAPK signaling. Thus, our results demonstrate that S332 is phosphorylated through a MAPK-dependent pathway, downstream of neuronal depolarization.

Phosphorylation of S332 regulates localization of ephrin-B3

We next asked whether phosphorylation of ephrin-B3 at S332 might control the subcellular localization of endogenous ephrin-B3. Consistent with a role for S332 in controlling ephrin-B3 localization in DIV21 cultured cortical neurons (Fig. 2f-h), pS332 ephrin-B3 was preferentially localized to dendritic shafts (Supplementary Fig. 5a, b; p<0.01, ANOVA). To address whether pS332 ephrin-B3 might have a similar distribution *in vivo*, brain sections from wild type and *Efnb3*$^{-/-}$ mice were stained with the pS332 antibody. In sections from wild type, but not *Efnb3*$^{-/-}$ mouse cortex, pS332 ephrin-B3 was enriched in apical dendrites of many layer 2/3 and 5 pyramidal neurons (Supplementary Fig. 3g). The subcellular localization of phosphorylated ephrin-B3 *in vivo* was determined by staining P14-15 pyramidal neurons filled with EGFP in cortical brain sections from wild-type and *Efnb3*$^{-/-}$ mice with the pS332 antibody (Fig. 3d, Supplementary Fig 3h). These experiments revealed that pS332 immunostaining is enriched in the dendritic shaft compared with the levels found in spines (Fig. 3d, f, p<0.05, ANOVA).

To confirm the role of S332 in the synaptic localization of ephrin-B3 *in vivo*, biochemical fractionation was used to generate synaptic fractions from P21-P23 mouse cortex [22,29]. Ephrin-B3 was enriched in PSD fractions together with PSD-95 and NMDA glutamate

receptor subunits (Fig. 3e, Supplementary Fig. 5c). In contrast, phosphorylated ephrin-B3 recognized by the ephrin-B3 pS332 antibody was significantly more abundant in solubilized synaptic plasma membranes (SPM-Tx, Fig. 3e, g, Supplementary Fig. 5c, p<0.05, t-test), indicating that phosphorylated ephrin-B3 is preferentially localized extra-synaptically. We observed similar enrichment of ephrin-B3 in synaptic fractions (P2, Syn) prepared from P21 mouse brain (Supplementary Fig. 5d). Moreover, probing with antibodies against total ephrin-B3 and pS332 ephrin-B3 demonstrated that phosphorylated ephrin-B3 was 80% less enriched in synaptosomes and 65% less enriched in P2 fractions compared to non-synaptic S1 fractions (Supplementary Fig. 5d-f p<0.0001, ANOVA). These experiments indicate that phosphorylation of S332, a site that is required for ephrin-B3 to interact with PSD-95, reduces levels of ephrin-B3 at synaptic sites.

Phosphorylation of S332 regulates localization of PSD-95

To begin to test whether S332 might be phosphorylated and regulate the synaptic localization of ephrin-B3 under physiological conditions, sensory information was deprived from barrel cortex in one hemisphere of P21 male mice by whisker trimming. Whisker trimming reduces neuronal activity in the deprived barrels [30]. After three days of deprivation, the barrel cortices of deprived and non-deprived hemispheres were collected and synaptosomes were purified (Fig. 3h). Consistent with the model, in synaptosomes from deprived barrel cortex the level of ephrin-B3 was significantly increased (Fig. 3i, k, Supplementary Fig. 5g, p<0.01, paired t-test) and the fraction of the total ephrin-B3 that was phosphorylated at pS332 was significantly decreased (Fig. 3i, l, Supplementary Fig. 5g, p<0.01, paired t-test). Levels of other synaptic proteins including CaMKII were unchanged (Fig. 3i). Thus, sensory deprivation leads to lower levels of phosphorylated ephrin-B3, likely driving the accumulation of ephrin-B3 at synapses.

Phosphorylation of S332 reduces the ability of ephrin-B3 to bind PSD-95. Therefore, we hypothesized that in deprived barrel cortex the ephrin-B3/PSD-95 interaction should be increased. Remarkably, whisker trimming led to a significant increase in the amount of PSD-95 that co-IP-ed with ephrin-B3 from deprived synaptosomes (Fig. 3j, m, Supplementary Fig. 5h, p<0.05, paired t-test). Overall, these results indicate that changes in sensory activity modulate ephrin-B3 phosphorylation *in vivo*, which regulates the localization of ephrin-B3 at synapses and its association with PSD-95.

Ephrin-B3 interacts with PSD-95 specifically at synaptic sites and appears to regulate the synaptic localization of PSD-95 in response to changes in sensory stimuli. To test whether this interaction is necessary for normal synaptic localization of PSD-95, we prepared synaptosomes from WT and *Efnb3*^{−/−} P10 and P21 mouse cortex during periods of rapid synaptogenesis (P10), and when synaptogenesis is largely complete (P21) [23,27]. Consistent with previous work, the expression level of PSD-95 in brain and the synaptic expression levels of CamKIIα, GluN2A and GluN2B were unchanged in the *Efnb3*^{−/−} animal [31,32] (Supplemental Fig. 6a-f). However, in synaptosomes isolated from *Efnb3*^{−/−} cortex at both P10 and P21, levels of PSD-95 normalized to synaptic CamKIIα were significantly lower than control (Fig. 4a, Supplementary Fig. 6g; p = 0.0458, t=3.298, df=3, P10 WT (n = 2 mice), P10 *Efnb3*^{−/−} (n = 3 mice) and p = 0.016, t=2.894, df=10, P21 WT (n = 6 mice), P2

Efnb3⁻/⁻,(n = 6 mice), unpaired two-tailed Student's t test). Similar results were found in PSD fractions prepared from P20-21 *Efnb3*⁻/⁻ cortex (Supplementary Fig. 7a-d, p<0.05, t-test). These results suggest that ephrin-B3 is necessary to maintain normal levels of PSD-95 at synapses.

Our *in vivo* data indicate that as early as P10, ephrin-B3 may be responsible for the proper localization of ~60% of the synaptic PSD-95. To determine whether the same domains of ephrin-B3 required for binding to PSD-95 are responsible for the synaptic localization of PSD-95, we prepared organotypic slice cultures from wild type and *Efnb3*⁻/⁻ mouse cortices and conducted molecular replacement experiments (Fig. 4b). We hypothesized that synaptic localization of PSD-95 would be rescued by ephrin-B3 mutants that promote the interaction with PSD-95 (Fig. 4b). Slices were prepared from P5-P7 animals and biolistically transfected with a construct expressing PSD-95-GFP and tdTomato to visualize PSD-95-GFP puncta and dendritic morphology, respectively. Three to five days following transfection, layer 2/3 and 5 cortical neurons were imaged with a two-photon microscope (Leica SP2 equipped with a 2.5W Mai-Ti DeepSee laser system) and the localization and distribution of PSD-95-GFP within primary and secondary branches of apical dendrites were determined (Fig. 4c, d).

In wild type brain slices, PSD-95-GFP was punctate and predominantly localized to dendritic spines adjacent to presynaptic specializations (Fig. 4c, filled arrowheads, Supplementary Fig. 8 a, b). Remarkably, in *Efnb3*⁻/⁻ neurons PSD-95-GFP fluorescence was found in a diffuse pattern throughout the dendritic arbor (Fig. 4c). The PSD-95-GFP fluorescence in the dendritic shaft likely represents freely diffusible or unbound PSD-95-GFP [9]. Consistent with this, the ratio of PSD-95-GFP fluorescence per pixel in PSD-95-GFP puncta to the average intensity in puncta-free regions of the dendritic shaft [16,33], was significantly higher in ephrin-B3 null neurons (Fig. 4e; p<0.0001, ANOVA). Single neuron rescue of ephrin-B3 expression caused the re-localization of PSD-95-GFP puncta from dendritic shafts to dendritic spines and rescued the diffuse dendritic PSD-95-GFP pattern (Fig. 4c, e, p<0.0001, ANOVA), indicating that the change in PSD-95-GFP was due to the loss of ephrin-B3 expression. These findings were phenocopied in single neuron knockdown and rescue of ephrin-B3 expression [22] in wild type brain slices (Fig. 4d, e; p<0.0001, ANOVA) and cultured neurons (Fig. 4f-k). Importantly, knockdown of EphB2, another *trans*-synaptic organizing protein known to regulate synapse formation [23], caused a significant (>40%) decrease in PSD-95-GFP puncta density, but did not alter the localization of PSD-95-GFP in the dendritic shaft (Supplementary Fig. 8c-g). Together these findings indicate that ephrin-B3 likely functions postsynaptically to regulate PSD-95-GFP localization cell autonomously.

Next, using a molecular replacement strategy in ephrin-B3 null brain slices, we tested the necessity and sufficiency of S332 for the localization of PSD-95 in cortical neurons. Using biolistics, ephrin-B3 expression was rescued by expressing either S332D or S332A ephrin-B3 constructs in cortical neurons of *Efnb3*⁻/⁻ brain slices. Remarkably, non-phosphorylatable S332A ephrin-B3, but not the phosphomimetic S332D ephrin-B3 mutant, rescued the pattern of PSD-95-GFP localization to that of control neurons (Fig. 4c, e; p<0.0001, one way ANOVA). These data are consistent with our structure function studies

(Fig 2.) and suggest that phosphorylation of S332 of ephrin-B3 acts to control localization or stabilization of PSD-95 at synaptic sites.

Ephrin-B3 functions upstream of PSD-95

Our results are consistent with a model in which ephrin-B3 functions upstream of PSD-95 to retain PSD-95 at synapses. We next tested whether PSD-95 is required to organize ephrin-B3 clusters at synapses. We transfected neurons at DIV0 with either wild type flag-eB3 and PSD-95 shRNA, or PSD-95 shRNA alone, and processed them for immunocytochemistry at DIV10 (Fig. 5a-c). Knockdown of endogenous PSD-95 decreased PSD-95 expression (Supplemental Fig 9a, b), and as expected, caused a significant reduction in synapse density (Fig. 5a, d, p<0.0001, t-test, Supplementary Fig. 9 c, d) and the density of vGlut1[+] puncta (Fig. 5b, c, h; p<0.05, t-test) compared to controls. However, unlike the effects of ephrin-B3 knockdown on PSD-95-GFP, PSD-95 knockdown had no effect on the puncta density of either flag-eB3 or endogenous ephrin-B3 found at synaptic sites (Fig. 5e, f, i). Thus, ephrin-B3 is still able to localize to sites of cell-cell contact marked by pre-synaptic vGlut1, even when PSD-95 expression is significantly reduced. Moreover, flag-ephrin-B3 remained punctate and did not become diffuse following knockdown of PSD-95 (Fig. 5g). Thus, PSD-95 is not required to organize ephrin-B3 or localize ephrin-B3 to synaptic sites, indicating that ephrin-B3 likely functions upstream of PSD-95.

Ephrin-B3 regulates PSD-95 stability at synapses

To test whether ephrin-B3 might control the stability of PSD-95 at synapses, we performed fluorescence recovery after photobleaching (FRAP) experiments (Fig. 6a). The baseline rate of PSD-95-GFP recovery one hour after photobleaching was appoximately 25% of the pre-bleach value (Fig. 6b, c, Supplementary Video 1, n = 6 neurons). Consistent with previous reports [10,11,34], recovery of PSD-95-GFP fluorescence reached a plateau by about 20 minutes. Therefore, in subsequent experiments the recovery of PSD-95-GFP fluorescence was followed for 20 minutes once every 20 seconds [8] (Fig. 6a).

We next determined the rate of turnover of PSD-95-GFP at functional synapses. Cultured cortical neurons transfected with PSD-95-GFP were loaded with FM4-64 dye to mark presynaptic release sites [35] and FRAP was determined for PSD-95-GFP puncta (Fig. 6d). Twenty minutes after bleaching, fluorescence recovery of PSD-95-GFP was similar for both synaptic and non-synaptic PSD-95 puncta (~20% of initial value, Fig. 6d-f; p = 0.0805, Kolmogorov-Smirnov (KS) nonparametric test).

Next, we asked whether knockdown of ephrin-B3 expression might change the stability of PSD-95-GFP. Knockdown of ephrin-B3 resulted in significantly higher levels of PSD-95-GFP fluorescence recovery at both synaptic (p<0.0001, KS test) and non-synaptic sites (Fig. 6d, e, Supplementary Video 2, p<0.0001, KS test). GFP intensity in ephrin-B3 shRNA transfected neurons recovered ~30% within the first five minutes of imaging and remained significantly higher than the control for the remainder of the 20 minutes of imaging (Fig. 6f, p<0.0001, ANOVA), indicating that ephrin-B3 knockdown results in a significantly higher mobile pool of PSD-95-GFP at both synaptic and non-synaptic sites. Interestingly, synaptic puncta recovered faster than non-synaptic puncta after ephrin-B3 knockdown (Fig. 6d-e; p =

0.0002, KS test). However, there was no difference in the mean fraction of recovery between synaptic and non-synaptic PSD-95-GFP puncta (Fig. 6f, p = 0.5 at 5 min, p = 0.2 at 18 min, ANOVA). Overall, these findings suggest that ephrin-B3 controls the mobility of a significant fraction of PSD-95 by regulating the rate of turnover or stabilization of PSD-95 at synaptic sites.

S332 of ephrin-B3 is required for the stability of PSD-95

Ephrin-B3 functions upstream of PSD-95 and regulates PSD-95 stability at synapses. We next sought to examine whether stabilization of PSD-95 by ephrin-B3 is regulated through the same domains that regulate PSD-95/ephrin-B3 interaction (Fig. 2) using FRAP combined with a molecular replacement strategy. Knockdown of ephrin-B3 significantly enhanced the recovery of bleached PSD-95-GFP (Fig. 7a, b; p<0.0001; KS test; Supplementary Video 3), resulting in an increased pool of mobile PSD-95-GFP (Fig. 7c, d, p<0.01 (5 min), p<0.05 (18min), ANOVA). Transfection of an shRNA-resistant wild type flag-eB3 construct rescued PSD-95-GFP recovery (Fig. 7a, b; p = 0.5185, K-S test) and the mobile fraction of PSD-95-GFP (Fig. 7c, d) back to control levels, indicating that increased PSD-95-GFP mobility is due to ephrin-B3 knockdown.

The ERK-binding domain and S332 in ephrin-B3 are required for the interaction between ephrin-B3 and PSD-95. To test whether the ephrin-B3 binding to PSD-95 might regulate PSD-95 mobility, we conducted molecular replacement studies. Neurons transfected with PSD-95-GFP, shRNA targeting ephrin-B3, and an shRNA resistant flag-eB3-L293A D-domain mutant failed to rescue either the diffusely distributed PSD-95-GFP (Supplementary Fig. 10a-c p<0.05, ANOVA), the increased turnover (Fig. 7a, e, p<0.0001, K-S test; Supplementary Video 3), or elevated mobile fractions of PSD-95-GFP (Fig. 7c, d, p<0.05 (5 min), p<0.01 (18 min), ANOVA). Indeed, the recovery of PSD-95-GFP fluorescence in neurons transfected with flag-eB3-L293A and ephrin-B3 shRNA was significantly higher than in ephrin-B3 shRNA only transfected neurons (Fig. 7e, p<0.047, KS test), suggesting that the L293A mutation may act as a dominant negative and suppress activity of endogenous ephrin-B3. Overall, these findings indicate that the ERK binding domain of ephrin-B3 is required for the stability of PSD-95 at synaptic sites.

To test whether phosphorylation of ephrin-B3 at S332 is necessary for the control of PSD-95 stability, we rescued ephrin-B3 expression with flag-eB3-S332D. Consistent with S332 phosphorylation acting negatively, neurons transfected with the phosphomimetic flag-eB3-S332D rescue construct had significantly higher PSD-95-GFP fluorescence intensity in dendritic shafts than control neurons (Supplementary Fig. 10a-c, p<0.001, ANOVA) and enhanced recovery of photo-bleached PSD-95-GFP puncta (Fig. 7a, f; p<0.0001, K-S test; Supplementary Video 3). Neurons transfected with shRNA resistant flag-eB3-S332D also had significantly higher levels of mobile PSD-95-GFP than controls (Fig. 7c, d, p<0.05 (5 min), p<0.01 (18 min), ANOVA). Importantly, the transfection of the non-phosphorylatable flag-ephrin-B3 mutant (flag-eB3-S332A) that can interact with PSD-95 rescued the distribution, (Supplementary Fig. 10a-c) recovery,(Fig. 7a, g; p=0.1196, K-S test) and mobile fractions of PSD-95 to control levels (Fig. 7c, d, p<0.01, ANOVA and Supplementary Video 3). Thus, the S332 residue in ephrin-B3 negatively regulates the

ephrin-B3 interaction with PSD-95 and is both necessary and sufficient to control PSD-95 stability.

MAP kinases are negative regulators of PSD-95 stability

Ephrin-B3 binding to ERK reduces ERK activity and prevents ERK translocation to the nucleus [22], while PSD-95 stability requires an intact D-domain in ephrin-B3. Additionally, ERK-dependent phosphorylation of S332 negatively regulates the ephrin-B3/PSD-95 interaction and PSD-95-GFP mobility. Therefore, we tested whether ERK activity may negatively regulate ephrin-B3 dependent PSD-95-GFP turnover.

To examine the role of ERK in ephrin-B3-dependent regulation of PSD-95-GFP turnover, we blocked the upstream ERK activator, MEK, using U0126 [28] and asked whether this might rescue PSD-95-GFP mobility to normal levels in ephrin-B3 shRNA transfected neurons (Fig. 8). FRAP experiments were conducted in single neurons transfected with PSD-95-GFP and either control or ephrin-B3 shRNA constructs before and after MEK inhibition. First, a single PSD-95-GFP puncta was bleached and its recovery determined. Then ERK activity was blocked with U0126 for 30 minutes, after which the mobility of a second PSD-95-GFP puncta in the same neuron was determined with FRAP.

Consistent with ERK playing a negative regulatory role, blockade of the MAPK pathway in wild type neurons significantly decreased the recovery of PSD-95-GFP (Fig. 8 a, b; p<0.0001, K-S test). Interestingly, inhibition of ERK did not change PSD-95-GFP mobility at early time points during recovery (Fig. 8c), but led to a significant reduction in the mobile pool of PSD-95-GFP at later time points (Fig. 8d, p<0.05, paired Student's t test), suggesting that ERK signaling might be particularly important in later phases of PSD-95 stabilization. Inhibition of ERK activity is also sufficient to restore PSD-95-GFP turnover within a neuron after knockdown of endogenous ephrin-B3, consistent with the idea that ERK is a negative regulator of PSD-95 turnover (Fig.8e-h; p<0.0001, K-S test, p<0.05 paired Student's t-test). Overall, our data are consistent with a model where ephrin-B3 controls the turnover rate of PSD-95 through its interaction with PSD-95 and by inhibiting ERK signaling.

Discussion

The precise localization and scaffolding activity of PSD-95 is essential for normal synaptic function and behavior [1,18]. Yet, how this intracellular synaptic organizer, PSD-95, is localized and maintained at the correct sites of cell-cell contact has remained poorly understood. In the present study we show that the synaptic localization and stability of PSD-95 in cortical neurons depends on a direct interaction with the *trans*-synaptic organizing protein ephrin-B3. Remarkably, ephrin-B3 appears to control the stability of the majority of PSD-95 at synaptic sites and links the stability of PSD-95 at synapses to changes in neuronal activity, including changes in sensory driven neuronal activity. The ephrin-B3/PSD-95 interaction, synaptic localization, and PSD-95 mobility are negatively regulated by MAPK activity and activity-dependent phosphorylation of ephrin-B3 on S332. Taken together, our findings provide the first example of a *trans*-synaptic negative regulatory signaling mechanism that stabilizes a key synaptic organizer, PSD-95, at synapses.

Regulation of synaptic localization of PSD-95

PSD-95 stabilizes proteins at the PSD that underlie synaptic function, plasticity, and development [1]. During experience dependent plasticity, PSD-95 appears to promote the delivery of AMPARs to synaptic sites [2,25,36] and changes in sensory driven neuronal activity alter the stability of PSD-95 at synaptic sites [9]. However the removal of PSD-95 binding partners, such as NMDARs and mGluRs, have little impact on the mobility or synaptic localization of PSD-95 [10], nor does the stability of PSD-95 at synapses appear to rely on intact actin cytoskeleton [8,10]. Moreover, post-translational modifications of PSD-95, such as palmitoylation and phosphorylation, affect PSD-95 stability by regulating its membrane incorporation but are not sufficient to explain the synaptic stability and localization of PSD-95 [13-16]. Indeed, it has been difficult to identify a molecule whose loss causes destabilization of PSD-95 at synapses. Our results identify a new interacting protein that localizes and stabilizes PSD-95 to synapses, regulates PSD-95 mobility and likely links changes in PSD-95 synaptic localization to neuronal activity. The ephrin-B3/PSD-95 interaction: 1) occurs selectively at synapses, 2) is direct, 3) is specific for ephrin-B3, and 4) is negatively regulated by the activity-driven MAPK-dependent phosphorylation of ephrin-B3 at S332. The observation that ephrin-B3 forms synaptically localized puncta after knockdown of PSD-95 indicates that ephrin-B3 acts upstream of PSD-95 to regulate PSD-95 turnover and stability, and suggests that ephrin-B3 may impact the organization of the synaptic scaffold as a whole by anchoring PSD-95 to synaptic sites.

Consistent with this model, PSD-95 knockout mice [37] and mice lacking ephrin-B3 have no apparent decrease in synapse number [22], but display reduced AMPAR/NMDAR EPSC ratio in the hippocampus [31], while *Efnb3*^{−/−} mice have defects in the synaptic localization of PSD-95. Given the similarities between the phenotypes of these knockouts, it is perhaps surprising that the ephrin-B3/PSD-95 interaction was not identified earlier. Unlike many interactions, binding of ephrin-B3 to PSD-95 is negatively regulated by phosphorylation and occurs only at synaptic sites *in vivo.* Thus, identification of this interaction was challenging in experiments that used whole cell extracts not enriched for synaptic components, which contain high levels of phosphorylated ephrin-B3, or in experiments that were enriched for phosphorylated synaptic proteins [38]. Indeed, we were unable to detect the co-IP of ephrin-B3 with PSD-95 in whole brain lysates. While mice lacking ephrin-B3 have reduced levels of synaptic PSD-95, additional proteins likely aid in organizing PSD-95 because some PSD-95 clusters form in the absence of ephrin-B3 [34,39,40]

Negative regulation of PSD-95 stability by MAPK

At many excitatory synapses, activation of post-synaptic NMDA type glutamate receptors by different patterns of synaptic activity induce increases or decreases in the strength of synaptic transmission [2]. Both the formation of new synapses and synaptic plasticity likely rely on modifications of PSDs and pre-synaptic terminals [41]. PSD-95 appears to be an important element that links changes in experience to changes in glutamate receptor number and synaptic strength [36]. Here we demonstrate that the activity-induced MAPK/ERK pathway, known to have important roles in LTP and learning [28], is linked to ephrin-B3 signaling and the control of PSD-95 stability. The functional significance of this interaction is indicated by the observation that sensory deprivation results in reduced levels of ephrin-

B3 S332 phosphorylation and increased association of PSD-95 in synaptic fractions. Strikingly, blocking ERK activity indicates that the MAPK pathway is a negative regulator of PSD-95 stability in neurons, and as such, activation of MAPKs might act to mobilize PSD-95. This negative regulatory function of ERK/MAPKs in controlling PSD-95 stability is consistent with the high degree of PSD-95 mobility observed during LTP-induced structural plasticity. By enabling enhanced PSD-95 mobility, ERK activation could allow for PSDs to undergo repositioning in spines and promote addition of PSD-95 to re-establish the steady-state composition of the PSD [42,43]. Consistent with this, loss of ephrin-B3 has been shown to disrupt various forms of plasticity associated with LTP and LTD [21,31,32]. Thus, phosphorylation of ephrin-B3 at S332 functions as an activity-regulated molecular switch controlling the stability and localization of PSD-95.

Implications for synapse density and stability

Overexpression of either PSD-95 or ephrin-B3 alone results in increased synapse density, while knockdown of either PSD-95 or ephrin-B3 expression reduces synapse density [3-5,22]. Interestingly, *Efnb3*^{−/−} mice have reduced density of dendritic spines, but exhibit normal density of synapses in cortex [22]. Thus, ephrin-B3 does not function as a classic synaptogenic molecule that is required for synapse assembly. Instead, relative levels of ephrin-B3 between neurons regulate overall synapse density in individual neurons [22], consistent with a *trans*-cellular competition that may govern synapse density in the developing cortex [44]. Because accumulation of PSD-95 at PSDs has been shown to be essential for regulating the stability of synaptic structures [3,33], but see [45], one attractive model suggested by our findings is that ephrin-B3 might regulate synapse density by controlling the stabilization or maintenance of synapses by direct stabilization of PSD-95 at synaptic sites or by negative regulation of ERK signaling. By enabling signaling between a *trans*-synaptic organizer and a scaffolding protein, ephrin-B3/PSD-95 interaction could play an important role in how neurons decide whether to accept or reject potential synaptic contacts. Consistent with this model, increased ERK signaling causes the breakdown of fixed, mature structures and emergence of de-novo filopodia [46]. Indeed, we observe that synapse density is reduced when ephrin-B3 is knocked down and is rescued by ephrin-B3 mutants that promote interaction with and stabilization of PSD-95 at synapses. Thus, ephrin-B3 may serve to integrate both positive synaptogenic signaling driven by PSD-95 and negative synaptic loss signaling driven by ERK signaling.

Implications for Plasticity

Homeostatic scaling of synaptic strength appears to rely on the bidirectional adjustments in synaptic AMPAR abundance driven by changes in the availability of MAGUKs such as PSD-95 and SAP-102 [47]. However, the molecular mechanisms driving activity-regulated changes in PSD-95 stability at synaptic sites have been more difficult to determine. The activity-regulated modulation of ephrin-B3/PSD-95 interaction provides an attractive molecular mechanism to regulate synaptic strength. Consistent with this model, sensory deprivation that results in homeostatic up-scaling of deprived inputs [48] reduced ephrin-B3 phosphorylation and enhanced the ephrin-B3/PSD-95 interaction. This mechanism could drive more PSD-95 to a subset of synapses, perhaps only those with reduced levels of neuronal activity. Consistent with the importance of ephrins in these events, in the *Drosophila* ephrin homologues are required for glutamate receptor dependent homeostatic

plasticity at the NMJ [49]. In the future, it will be important to determine how the ephrin-B3/ PSD-95 interaction might be linked to abnormal changes in synapse numbers and morphology associated with disease states such as epilepsy and ASD [50].

Methods

Animals

All animal studies were performed according to the Institutional Animal Care and Use Committee guidelines at Thomas Jefferson University. Wild type and ephrin-B3 null littermates were generated and genotyped as described previously [22,51,52]. E17-18 time pregnant rats and wild type CD-1 male mice used for whisker trimming were purchased from Charles River Laboratories Inc. (Wilmington, MA).

Sensory Deprivation

CD-1 P21 wild type males were anesthetized with 4% isoflurane using isoflurane vaporizer (VSS, Rockmart, GA). All facial vibrissae on the right side were trimmed leaving the left side untouched. Trimming was done every 24 hours for 3 days while maintaining the animals in standard (un-enriched) conditions. After 72 hours of sensory deprivation, animals were sacrificed, barrel cortices from deprived and non-deprived (control) hemispheres were rapidly dissected and flash frozen in liquid nitrogen. The tissue was used for synaptosomal preparation and biochemical analysis.

Cortical neuronal and organotypic slice cultures

Dissociated cortical neurons were prepared from embryonic day 17-18 (E17-18) rat cerebral cortex as described previously [22,23] and cultured in Neurobasal (Invitrogen, Carlsbad, CA) supplemented with B27 (Invitrogen), glutamine (Sigma, St. Louis, MO) and penicillin-streptomycin (Sigma) on poly-D-lysine (BD Biosciences, San Jose, CA) and laminin (BD Biosciences) coated glass coverslips (12 mm; Bellco Glass, Vineland, NJ). Neurons were plated at 150,000/well in 24-well plates for transfection experiments and were maintained in a humidified 37ºC incubator with 5% CO_2. For organotypic cortical brain slices, 300 μm slices were made from postnatal day 4 (P4) to P6 wild type or $Efnb3^{-/-}$ mice using a vibratome (Warner Instruments, Hamden, CT). Slices were cultured in 0.4 μm Millicell culture inserts (Millipore, Bedford, MA) in six-well plates [23,27]. Slices were maintained in a humidified 37ºC incubator with 5% CO_2 in 750 μl of medium containing 50 ml Neurobasal with B27 supplement, 25 ml of Hank's Balanced Salt Solution (HBSS, Invitrogen), 25 ml of heat-inactivated horse serum (Invitrogen), 0.65 g of dextrose (Sigma), 1 ml of 1M HEPES, pH 7.0 (Invitrogen) and 1 ml of penicillin-streptomycin, at pH 7.2. $Efnb3^{-/-}$ mice were generated and outcrossed into CD1 background by Dr. Mark Henkemeyer (University of Texas Southwestern Medical Center, Dallas, TX) [52].

Depolarization of neurons with KCl

DIV14 rat cortical neurons were treated with TTX (1 μM, Tocris) for four hours at 37 ºC to inhibit action potentials and bring the overall levels of neuronal activity to baseline. To block ERK activation, some wells were treated for four hours with either U0126 (10 μM, Sigma) or PD98059 (100 μM, Sigma) MEK inhibitors [28] along with TTX. After four hours,

neuronal activity was elevated by depolarizing neurons with 55 mM KCl for one hour at 37 °C [53] in the presence of TTX and either the presence or absence of MEK inhibitors. After one hour, neurons were immediately lysed with boiling 6x sample buffer, separated by SDS-PAGE and processed for western blot analysis.

cDNA and shRNA constructs

PSD-95-GFP, all FLAG tagged ephrin-B3 constructs and ephrin-B3 shRNA constructs used for transfections and biochemistry experiments have been previously generated and characterized in the Dalva lab [22,23,27,51]. For neuronal transfections, we cloned wild type and mutant ephrin-B3 cDNAs into a pENTR4 plasmid that contains the neuronal specific synapsin promoter (kindly provided by Dr. Peter Scheiffele, University of Basel, Biozentrum). For cortical slice transfections, we used a GATEWAY technology approach (Invitrogen) to generate constructs to drive simultaneous expression of PSD-95-GFP, tdTomato and ephrin-B3 shRNA or control pSuper cassette from human ubiquitin (hUb), synapsin (Syn) and H1 promoters, respectively. To do this, we have converted an existing pFUGW vector [54] into a GATEWAY destination vector using a Gateway vector conversion system kit (Invitrogen). First, we removed GFP downstream of the hUb promoter from the original pFUGW by cutting with XbaI (New England Biolabs) and subsequently blunted the sites with Klenow fragment (New England Biolabs). Then in place of GFP we cloned Reading Frame A cassette (RfA, Invitrogen) that contains 5' attR1 and 3' attR2 sites, with chloramphenicol and *ccdB* genes, thus rendering the pFUGW vector Gateway compatible. Finally, to generate the expression plasmid containing PSD-95, tdTomato and ephrin-B3 shRNA with their respective promoters, we performed 4-fragment Gateway LR recombination by combining the pFUGW-Destination vector and four pDONR 221 entry plasmids containing the following fragments: 1) 5' attL1_PSD-95-GFP_attR5 3'; 2) 5' attL5_BGH_PA_attL4 3'; 3) 5' attR4_SynPro_tdTomato_SV40PA_attR3r 3' and 4) 5' attL3_H1_ephrin-B3shRNA_attL2 3' or 5' attL3_pSuper cassette_attL2 3'. The resulting pFUGW expression plasmids contained PSD-95-GFP under control of hUb promoter, tdTomato under control of the Synapsin promoter and ephrin-B3 shRNA or pSuper cassette under control of the H1 promoter.

Constructs containing ephrin-B3 cytoplasmic domains that were used for *in vitro* translation were generated by cloning the sequence corresponding to amino acids 249-340 of mouse ephrin-B3 (uniprot.org) into the EcoRI and XhoI sites of the pT7CFE-NHis vector (cat#: 88859, Thermo-Fisher Scientific). The flag-tag sequence was added to the 5' end of all intracellular ephrin-B3 sequences to enable efficient purification and detection. PCR using the high fidelity Phusion Flash polymerase (cat#: F-548L, Thermo-Fisher Scientific) was used to generate flag-tagged ephrin-B3 intracellular fragments containing 5' EcoRI and 3' XhoI sites with following primers: Forward primer: 5' ATGAATTCATCGATGACTACAAGGACGACGATGACAAGATGTGTTGGCGGAGACG GCGGGCCA 3', and Reverse primer: 5' agctcgagTCATACCTTGTAATAGATGTTCGG 3'.

Transfection of neuronal and slice cultures

For all transfection experiments neurons were transfected at day *in vitro* 0 (DIV0) in suspension using Lipofectamine 2000 (Invitrogen) [23,55] and processed for imaging at 9-10

DIV for fluorescence recovery after photobleaching (FRAP) imaging or at DIV 10-21 for immunostaining. Cortical slices were transfected using a Helios Gene Gun (Bio-Rad, Hercules, CA) as described previously [23]. DNA constructs encoding either the PSD-95-GFP/tdTomato/ephrin-B3 shRNA or PSD-95-GFP/tdTomato/pSuper cassette with or without wild type rescue flag-tagged ephrin-B3 were coated onto 5mg of 1.6 μm gold particles in a solution with 0.01 mg/ml PVP, 0.05 M spermidine, 1 M $CaCl_2$ and H_2O. The solution was drawn into tubing and coated to the sides. The tubing was cut into cartridges, loaded into the Gene Gun and gold particles were shot with high-pressure helium (120-130 psi) into cultured slices in inserts sitting on warm 1.6% agarose plates. Slices were imaged live using a two-photon laser scanning microscope 4 days after transfection. Transfection of HEK 293T cells was performed using a calcium phosphate precipitation method as described previously [23]. HEK 293T cells were used for co-immunoprecipitation or western blot analysis with indicated antibodies 24 hours after transfection.

Antibodies and Reagents

For the generation of a phospho-specific S332 (pS332) antibody that recognizes phosphorylated ephrin-B3 S332, three rabbits were subcutaneously injected (Covance, Princeton, NJ) with custom-synthesized KLH-conjugated pS332 peptide (IVQDGPPQ-pS-PPNIYYKV, EZBiolab, Inc., Carmel, IN). The antibody was affinity purified from rabbit sera using the pS332 peptide and tested for specificity in biochemical and imaging preparations (Supplementary Fig. 2). In all subsequent experiments pS332 (rabbit antisera 1178) was used at 1:4000 for western blotting and (rabbit antisera 1176) was used at 1:2000 for immunocytochemistry and immunohistochemistry.

Primary antibodies: mouse monoclonal α-PSD-95 clone K28/43 (1:1000, Neuromab, UC Davis, Davis, CA, clone 28/43), α-PSD-95 (1:2000, Thermo Fisher Scientific, Pittsburgh, PA, cat#: MA1-046), α-M2 FLAG (1:1000, Sigma, Saint Louis, MO, cat#: F3165), α-pan-ephrin-B (1:1000, Thermo Fisher Scientific, cat#: 37-8100), α-Glycerlaldehyde-3-Phosphate Dehydrogenase (GAPDH, clone 6C5, 1:500, Milipore, Temecula, CA, cat#: MAB374), α-GluN2B clone N59/36 (1:300, Neuromab); rabbit polyclonal α-CaMKIIα (1:1000, Cell Signaling, Danvers, MA, cat#: 3357) α-FLAG (1:1000, Sigma, cat#: F7425), α-ephrin-B3 (1:100, Thermo Fisher Scientific, extracellular epitope, cat#: 34-3600), α-ephrin-B3 (1:250, Santa Cruz Biotechnology, Santa Cruz, CA, Intracellular epitope, cat#: sc20724), α-GluN2A (1:1000, Millipore, cat#: 07-632); rabbit monoclonal α-phospho-p44/p42 MAPK (Erk1/2, Thr202/Tyr204; 1:1000, Cell Signaling, cat#: 4695), α-p44/p42 MAPK (Erk1/2; 1:1000, Cell Signaling, cat#: 4377); goat polyclonal α-ephrin-B1 (1:500, R&D Systems, Minneapolis, MN, cat#: AF473), α-ephrin-B2 (1:500, R&D Systems, cat#: AF496); guinea pig polyclonal α-vesicular glutamate transporter 1 (α-vGlut1; 1:5000, Milipore, cat#: AB5905).

Secondary antibodies—Highly pre-adsorbed αmouse, αrabbit DyLight 488 and αguinea pig 649 were obtained from Jackson ImmunoResearch (West Grove, PA) and used at 1:500. Anti-mouse and αrabbit Atto 425 conjugated secondary antibody was obtained from Rockland, Inc. (Gilbertsville, PA) and used at 1:250. Horseradish peroxidase

conjugated secondary antibodies (αmouse and αrabbit) were obtained from Jackson ImmunoResearch and used at 1:20,000.

Immunocytochemistry and immunohistochemistry

Dissociated cortical neurons were fixed at indicated times in 4% paraformaldehyde (PFA)/2% sucrose in PBS for 8 minutes at room temperature. Neurons were then washed three times in PBS, blocked and permeabilized for 2 hours at room temperature in 1% ovalbumin, 0.2% gelatin from cold-water fish in PBS containing 0.01% saponin. Neurons were then stained for 2 hours at room temperature with indicated primary antibodies, washed three times in PBS and then immunostained with corresponding secondary antibodies for 45 min at room temperature. After washing three times in PBS, coverslips were mounted with MOWIOL and used either for the conventional confocal or stimulated emission depletion (STED) imaging.

For immunohistochemistry, P10-16 mice were perfused trans-cardially with PBS followed by 4% PFA. The brains were removed and post-fixed overnight in 4% PFA at 4°C. 30 μm sections were then made using a VT-1000S vibratome, permeabilized for 25 min at room temperature in PBS containing 0.5% saponin, then blocked overnight at 4°C in PBS containing 0.1% saponin, 10% horse serum and 1% BSA. Sections were then incubated overnight at 4°C in blocking solution containing indicated primary antibodies after which they were washed three times for 10 mins in PBS and incubated for 2 hours at room temperature with blocking solution containing indicated secondary antibodies. Sections were then washed three times for 10 mins PBS and mounted with aquamount mounting media.

Organotypic slice IHC—Biolistically transfected slices were fixed by submersion in 4% PFA+0.1% glutaraldehyde for 30 minutes at room temperature. The fixed slices were removed from the culture plate membranes and washed three times for 10 minutes in PBS, then submerged in 30% sucrose/PBS overnight at 4°C. All further steps were carried out with the sections free-floating. The slices were then re-sectioned at 30-50 μm using a sliding microtome, permeabilized for 25 minutes at room temperature in PBS containing 0.5% Triton X-100 (except for ephrin-B3 staining for which we used 0.5% saponin), then blocked overnight at 4°C in PBS containing 10% horse serum, 1% BSA and 0.2% triton X-100 (except for ephrin-B3 staining for which we used 0.1% saponin). For primary immunostaining, rabbit α-GFP and guinea pig α-vGlut1 antibodies were both used at 1:2500, and sections were incubated overnight at 4°C. The sections were then washed three times for 10 minutes in PBS and incubated with the indicated secondary antibodies for 2 hours at room temperature. The sections were washed three times for 10 minutes in PBS, and mounted with aquamount mounting media.

Post-synaptic Density and Synaptosomes

Post-synaptic densities were prepared by biochemical fractionation of cortical hemispheres from wild type and *Efnb3*^{−/−} littermates as described previously [29]. Synaptosomes were prepared from P10 and P21 wild type and *Efnb3*^{−/−} mice as previously described [22]. Briefly, brains were homogenized on ice in 0.32 M Sucrose, 4mM HEPES, pH7.4, containing protease inhibitor cocktail (Sigma) and 1mM PMSF. After removing the nuclear fraction by

centrifuging at 1000g for 15 minutes at 4ºC, S1 fractions were further centrifuged at 10,000g at 4ºC to obtain P2 fraction. Purified synaptosomes were obtained by centrifuging P2 through a gradient of 1) 1.2M sucrose and 2) 0.8M sucrose.

Immunoprecipitation

Synaptosomal pellets were resuspended and homogenized in lysis buffer (50mM Tris, 140mM NaCl, 0.5% NP40, pH7.4) containing general protease inhibitor cocktail (Sigma) and 1mM PMSF and phosphatase inhibitors (2mM EGTA (Sigma), 50mM NaF (Sigma), 1mM Na_3VO_4 (Sigma), 10mM $Na_4O_7P_2.10H_2O$ (Sigma) and 0.1 mM $H_{24}Mo_7N_6O_{24}.4H_2H$ (Sigma). HEK 293T cells were lysed in 50mM Tris, 140mM NaCl, 10mM NaF, 1mM Na_3VO_4, 1% NP40, pH7.4. Insoluble material was removed by centrifuging at 10,000 g for 20 minutes at 4ºC and the remaining supernatant was immunoprecipitated with indicated antibodies for 4 hours at 4ºC. Then 20µl of protein G beads (blocked in 1% BSA in lysis buffer) was added to the supernatant and incubated for an additional hour at 4ºC. Beads were washed three times with lysis buffer and once with Tris-buffered saline containing 10mM NaF, 1mM Na_3VO_4 with protease inhibitor cocktail (Sigma) and 1mM PMSF. Proteins were subsequently eluted from the beads by boiling in 4x SDS sample buffer for 5 minutes. Eluted proteins were separated on SDS-PAGE gels, transferred to PVDF membrane (Milipore), blocked with 5% milk, labeled with the indicated primary and HRP-conjugated secondary antibodies, and visualized with Western Lightning® Plus-ECL (PerkinElmer, Waltham, MA). In HEK 293T cell co-IP experiments, we performed densitometric analysis to determine the level of co-immunoprecipitated protein. To account for the differences in protein expression we normalized the amount of co-immunoprecipitated proteins to the amount of each construct present in the lysate in each of six experiments conducted.

Pull Down assay

Cloned intracellular ephrin-B3 fragments were used to generate flag-tagged ephrin-B3 cytosolic domains using the cell-free HeLa *in vitro* translation system (Invitrogen). Cytosolic ephrin-B3 domains were purified by incubating with flag antibody bound protein-G beads for one hour at 4ºC in binding buffer (50 mM Tric-HCl, 140 mM NaCl and 0.5% NP-40, pH 7.5) including protease inhibitor cocktail (Sigma) and 1 mM PMSF. After washing three times with binding buffer, 160 ng of recombinant PSD-95-GST (Novus Biologicals, Littleton, CO) was subsequently added to the mixture and incubated an additional hour at 4ºC with gentle agitation. Beads were then washed three times in binding buffer and bound complexes were eluted by boiling in 4x SDS protein sample buffer. We measured the amount of PSD-95-GST in pull down experiments and normalized it to baseline levels of PSD-95-GST found in no DNA controls.

Imaging and analysis

Cortical neuronal cultures were imaged by confocal scanning microscopy with a Leica TCS SP5 and Leica TCS STED CW confocal microscope (Leica Microsystems, Mannheim, Germany). For conventional confocal microscopy, images were acquired with a 63x oil immersion objective (Leica) at 1.7-1.9x zoom and were z-projections of 4-10 images taken at 0.3 µm step intervals. For STED imaging, images were acquired with 100x oil immersion

objective (Leica) with 5-10x zoom to obtain 15-30 nm pixel sizes and were single optical sections.

Imaging of fixed brain sections and re-sectioned organotypic brain slices was conducted with a Leica TCS SP5 CW confocal microscope. Images were acquired with a 63x oil immersion objective. For analysis of pS332 staining, stacks of images were taken at 0.3-.5 μm intervals and analyzed in ImageJ with experimenter blinded to condition. For analysis of PSD-95-GFP/vGlut1 colocalization, images from at least two independent experiments per condition were taken at 0.25 μm intervals and analyzed in ImageJ with the experimenter blinded to condition.

Fluorescence recovery after photobleaching experiments were conducted with a Leica TCS SP2 confocal scanning microscope (Leica). Cultured neurons on coverslips were removed from the culture dish, placed in an imaging chamber with artificial CSF (ACSF) and imaged using a 40x water immersion lens (Leica) at 1.9x zoom with 488 nm laser at 25% power. For bleaching, selected puncta were zoomed 32x and bleached with 5 scans of a 488 nm laser at 100% intensity. Images were single optical sections acquired every 20 seconds for 20 minutes or every 60 seconds for 1 hour. For FRAP of synaptic and non-synaptic PSD-95-GFP puncta, neurons were loaded with FM4-64 dye for 15 minutes using spontaneous loading as described [35] and then washed for 15 minutes with three 5-minute washes of ACSF before imaging with a Leica TCS SP5 confocal microscope. For these experiments, bleaching of PSD-95-GFP puncta colocalized with and not colocalized with FM4-64 puncta was performed by the Leica bleach points algorithm associated with a Leica TCS SP5 confocal microscope using 50 msec pulses of a 488 nm laser line set at 100% power.

For brain slices, cultured cortical slices were removed from the culture dish, placed into ACSF and imaged on a two-photon Leica TCS SP2 confocal microscope equipped with Mai Tai – series mode-locked titanium:sapphire laser tuned to 930 nm, pumped by a 12.5 W solid-state CW 532 nm laser source (Spectra Physics, Fremont, CA). Images are z-projections of 20-60 images taken at 0.5 μm intervals with HCX IRAPO L 25x/0.95 W lens. Images were analyzed in NIH ImageJ using built in plugins and custom made macros.

Fluorescence recovery after photobleaching analysis—GFP intensity of bleached puncta and four randomly selected unbleached puncta was quantified for each time point by selecting the regions of interest (ROIs) around selected puncta in every image in the time series. Four unbleached puncta served as a control for the bleaching that occurred during image acquisition and the recovery of bleached GFP puncta was normalized to the average intensity of unbleached puncta at each time point. The kinetics of bleached puncta recovery (represented as GFP intensity) were then determined by calculating the ratio of GFP fluorescence change over time to the GFP fluorescence before photobleaching using the $(F-F_0)/F_{pre}$ equation, where F is the GFP fluorescence measured at different time intervals, F_0 is the GFP fluorescence immediately after photobleaching at $t = 0$ sec and F_{pre} is the GFP fluorescence intensity before photobleaching.

Puncta co-clustering analysis—Analyses were performed blind to condition. Puncta co-clusters were analyzed using automated *ImageJ* custom-built macros, as described

previously [22,23,51]. Briefly, each channel was thresholded with the same value across experimental conditions and converted to a binary image. Puncta were defined as continuous pixels of 0.5-7.5 μm along at least 50 μm of dendrite and co-clustering as >1 pixel of overlap between the channels.

Puncta and dendritic shaft fluorescence analysis—For the cultured neurons transfected with PSD-95-GFP or tdTomato and flag-tagged ephrin-B3 constructs and for the wild type and *Efnb3*^{−/−} neurons in organotypic cortical slices transfected with tdTomato/PSD-95-GFP construct, average puncta pixel intensity per cell was determined by thresholding GFP or flag intensities in puncta along at least 50 μm of tdTomato labeled dendrite. Thresholded puncta intensities were then subtracted from the whole cell, leaving behind dendritic segments without puncta. Subtracted dendrites were re-thresholded to new values and the regions of interests (ROIs) were drawn around dendritic segments that enabled calculating shaft fluorescence values between subtracted puncta. Calculating the ratios of average shaft to average puncta intensities per cell basis was used to quantify relative amounts of PSD-95-GFP and flag-tagged ephrin-B3 in different subcellular compartments.

STED puncta analysis in dendritic spines—Super-resolution analysis was performed on DIV21 neurons transfected with tdTomato, ephrin-B3 shRNA and flag-tagged ephrin-B3 S332 mutant constructs or in wild type neurons transfected with tdTomato only. Dendritic spine localization of ephrin-B3 and PSD-95 was performed on a per spine basis. Spines were identified individually by thresholding tdTomato and drawing ROIs around the spine head. Spine localization of ephrin-B3 puncta and PSD-95 was determined by examining co-localization between thresholded PSD-95, ephrin-B3 or flag immunostaining and tdTomato in the selected regions. Synaptic localization was measured as co-localization with vGlut1 clusters, which were imaged in conventional resolution (~250 nm). Analysis was performed blind to transfection condition. Puncta counted were restricted by size as described above.

Statistical Analyses

Data are expressed as means ± sem. Statistical significance of differences among groups was determined by one-way analysis of variance followed by *post-hoc* test described in individual figure legends, or with *t*-test. Distribution of the data was assumed to be normal, but this was not formally tested. No statistical methods were used predetermine sample sizes, but our sample sizes are similar to those reported in previous publications [22,23,27,51]. Non-parametric Kolmogorov-Smirnov test was used to determine statistical significance of PSD-95-GFP puncta recovery for the FRAP experiments. Probability values of less than 5% were considered statistically significant. Unless stated otherwise, statistical measures were conducted on a per cell basis, collected from a minimum of three independent experiments. A supplementary methods checklist is available.

Supplementary Material

Refer to Web version on PubMed Central for supplementary material.

Acknowledgements:

References

1. Feng W, Zhang M. Organization and dynamics of PDZ-domain-related supramodules in the postsynaptic density. Nature reviews. Neuroscience. 2009; 10:87–99. doi:10.1038/nrn2540. [PubMed: 19153575]

2. Huganir RL, Nicoll RA. AMPARs and synaptic plasticity: the last 25 years. Neuron. 2013; 80:704–717. doi:10.1016/j.neuron.2013.10.025. [PubMed: 24183021]

3. Ehrlich I, Klein M, Rumpel S, Malinow R. PSD-95 is required for activity-driven synapse stabilization. Proceedings of the National Academy of Sciences of the United States of America. 2007; 104:4176–4181. doi:10.1073/pnas.0609307104. [PubMed: 17360496]

4. Elias G, Nicoll R. Synaptic trafficking of glutamate receptors by MAGUK scaffolding proteins. Trends in cell biology. 2007; 17:343–352. doi:10.1016/j.tcb.2007.07.005. [PubMed: 17644382]

5. El-Husseini A, Schnell E, Chetkovich D, Nicoll R, Bredt D. PSD-95 involvement in maturation of excitatory synapses. Science (New York, N.Y.). 2000; 290:1364–1368.

6. Bayés A, et al. Characterization of the proteome, diseases and evolution of the human postsynaptic density. Nature neuroscience. 2011; 14:19–21. doi:10.1038/nn.2719. [PubMed: 21170055]

7. Grant S. Synaptopathies: diseases of the synaptome. Current opinion in neurobiology. 2012; 22:522–529. doi:10.1016/j.conb.2012.02.002. [PubMed: 22409856]

8. Blanpied T, Kerr J, Ehlers M. Structural plasticity with preserved topology in the postsynaptic protein network. Proceedings of the National Academy of Sciences of the United States of America. 2008; 105:12587–12592. doi:10.1073/pnas.0711669105. [PubMed: 18723686]

9. Gray N, Weimer R, Bureau I, Svoboda K. Rapid redistribution of synaptic PSD-95 in the neocortex in vivo. PLoS biology. 2006; 4 doi:10.1371/journal.pbio.0040370.

10. Kuriu T, Inoue A, Bito H, Sobue K, Okabe S. Differential control of postsynaptic density scaffolds via actin-dependent and -independent mechanisms. The Journal of neuroscience : the official journal of the Society for Neuroscience. 2006; 26:7693–7706. doi:10.1523/jneurosci. 0522-06.2006. [PubMed: 16855097]

11. Sturgill J, Steiner P, Czervionke B, Sabatini B. Distinct domains within PSD-95 mediate synaptic incorporation, stabilization, and activity-dependent trafficking. The Journal of neuroscience : the official journal of the Society for Neuroscience. 2009; 29:12845–12854. doi:10.1523/jneurosci. 1841-09.2009. [PubMed: 19828799]

12. Ho G, et al. S-nitrosylation and S-palmitoylation reciprocally regulate synaptic targeting of PSD-95. Neuron. 2011; 71:131–141. doi:10.1016/j.neuron.2011.05.033. [PubMed: 21745643]

13. Nelson C, Kim M, Hsin H, Chen Y, Sheng M. Phosphorylation of Threonine-19 of PSD-95 by GSK-3β is Required for PSD-95 Mobilization and Long-Term Depression. The Journal of neuroscience : the official journal of the Society for Neuroscience. 2013; 33:12122–12135. doi: 10.1523/jneurosci.0131-13.2013. [PubMed: 23864697]

14. Steiner P, et al. Destabilization of the postsynaptic density by PSD-95 serine 73 phosphorylation inhibits spine growth and synaptic plasticity. Neuron. 2008; 60:788–802. doi:10.1016/j.neuron. 2008.10.014. [PubMed: 19081375]

15. Kim M, et al. Synaptic accumulation of PSD-95 and synaptic function regulated by phosphorylation of serine-295 of PSD-95. Neuron. 2007; 56:488–502. doi:10.1016/j.neuron. 2007.09.007. [PubMed: 17988632]

16. Craven S, El-Husseini A, Bredt D. Synaptic targeting of the postsynaptic density protein PSD-95 mediated by lipid and protein motifs. Neuron. 1999; 22:497–509. doi:10.1016/ s0896-6273(00)80705-9. [PubMed: 10197530]

17. Biederer T, Stagi M. Signaling by synaptogenic molecules. Current opinion in neurobiology. 2008; 18:261–269. doi:10.1016/j.conb.2008.07.014. [PubMed: 18725297]

Author Manuscript Author Manuscript Author Manuscript Author Manuscript

18. Zheng C-Y, Seabold G, Horak M, Petralia R. MAGUKs, synaptic development, and synaptic plasticity. The Neuroscientist : a review journal bringing neurobiology, neurology and psychiatry. 2011; 17:493–512. doi:10.1177/1073858410386384.

19. Mah W, et al. Selected SALM (synaptic adhesion-like molecule) family proteins regulate synapse formation. The Journal of neuroscience : the official journal of the Society for Neuroscience. 2010; 30:5559–5568. doi:10.1523/jneurosci.4839-09.2010. [PubMed: 20410109]

20. Shipman S, et al. Functional dependence of neuroligin on a new non-PDZ intracellular domain. Nature neuroscience. 2011; 14:718–726. doi:10.1038/nn.2825. [PubMed: 21532576]

21. Hruska M, Dalva M. Ephrin regulation of synapse formation, function and plasticity. Molecular and cellular neurosciences. 2012; 50:35–44. doi:10.1016/j.mcn.2012.03.004. [PubMed: 22449939]

22. McClelland A, Hruska M, Coenen A, Henkemeyer M, Dalva M. Trans-synaptic EphB2-ephrin-B3 interaction regulates excitatory synapse density by inhibition of postsynaptic MAPK signaling. Proceedings of the National Academy of Sciences of the United States of America. 2010; 107:8830–8835. doi:10.1073/pnas.0910644107. [PubMed: 20410461]

23. Kayser M, McClelland A, Hughes E, Dalva M. Intracellular and trans-synaptic regulation of glutamatergic synaptogenesis by EphB receptors. The Journal of neuroscience : the official journal of the Society for Neuroscience. 2006; 26:12152–12164. doi:10.1523/jneurosci.3072-06.2006. [PubMed: 17122040]

24. Chen X, et al. PSD-95 is required to sustain the molecular organization of the postsynaptic density. The Journal of neuroscience : the official journal of the Society for Neuroscience. 2011; 31:6329–6338. doi:10.1523/jneurosci.5968-10.2011. [PubMed: 21525273]

25. Hafner A-SS, et al. Lengthening of the Stargazin Cytoplasmic Tail Increases Synaptic Transmission by Promoting Interaction to Deeper Domains of PSD-95. Neuron. 2015; 86:475–489. doi:10.1016/j.neuron.2015.03.013. [PubMed: 25843401]

26. Wollscheid B, et al. Mass-spectrometric identification and relative quantification of N-linked cell surface glycoproteins. Nat Biotechnol. 2009; 27:378–386. doi:10.1038/nbt.1532. [PubMed: 19349973]

27. Kayser M, Nolt M, Dalva M. EphB receptors couple dendritic filopodia motility to synapse formation. Neuron. 2008; 59:56–69. doi:10.1016/j.neuron.2008.05.007. [PubMed: 18614029]

28. Thomas G, Huganir R. MAPK cascade signalling and synaptic plasticity. Nature reviews. Neuroscience. 2004; 5:173–183. doi:10.1038/nrn1346. [PubMed: 14976517]

29. Lau LF, et al. Interaction of the N-methyl-D-aspartate receptor complex with a novel synapse-associated protein, SAP102. The Journal of biological chemistry. 1996; 271:21622–21628. [PubMed: 8702950]

30. Holtmaat A, Svoboda K. Experience-dependent structural synaptic plasticity in the mammalian brain. Nature reviews. Neuroscience. 2009; 10:647–658. doi:10.1038/nrn2699. [PubMed: 19693029]

31. Antion M, Christie L, Bond A, Dalva M, Contractor A. Ephrin-B3 regulates glutamate receptor signaling at hippocampal synapses. Molecular and cellular neurosciences. 2010; 45:378–388. doi:10.1016/j.mcn.2010.07.011. [PubMed: 20678574]

32. Rodenas-Ruano A, Perez-Pinzon M, Green E, Henkemeyer M, Liebl D. Distinct roles for ephrinB3 in the formation and function of hippocampal synapses. Developmental biology. 2006; 292:34–45. doi:10.1016/j.ydbio.2006.01.004. [PubMed: 16466709]

33. Cane M, Maco B, Knott G, Holtmaat A. The relationship between PSD-95 clustering and spine stability in vivo. J Neurosci. 2014; 34:2075–2086. doi:10.1523/JNEUROSCI.3353-13.2014. [PubMed: 24501349]

34. Yoshii A, Constantine-Paton M. BDNF induces transport of PSD-95 to dendrites through PI3K-AKT signaling after NMDA receptor activation. Nature neuroscience. 2007; 10:702–711. doi:10.1038/nn1903. [PubMed: 17515902]

35. Wilhelm BG, Groemer TW, Rizzoli SO. The same synaptic vesicles drive active and spontaneous release. Nature neuroscience. 2010; 13:1454–1456. doi:10.1038/nn.2690. [PubMed: 21102450]

36. Ehrlich I, Malinow R. Postsynaptic density 95 controls AMPA receptor incorporation during long-term potentiation and experience-driven synaptic plasticity. The Journal of neuroscience : the

official journal of the Society for Neuroscience. 2004; 24:916–927. doi:10.1523/jneurosci. 4733-03.2004. [PubMed: 14749436]

37. Migaud M, et al. Enhanced long-term potentiation and impaired learning in mice with mutant postsynaptic density-95 protein. Nature. 1998; 396:433–439. doi:10.1038/24790. [PubMed: 9853749]

38. Fernández E, et al. Targeted tandem affinity purification of PSD-95 recovers core postsynaptic complexes and schizophrenia susceptibility proteins. Molecular systems biology. 2008; 5:269. doi: 10.1038/msb.2009.27.

39. Barrow S, et al. Neuroligin1: a cell adhesion molecule that recruits PSD-95 and NMDA receptors by distinct mechanisms during synaptogenesis. Neural development. 2009; 4:17. doi: 10.1186/1749-8104-4-17. [PubMed: 19450252]

40. Giannone G, et al. Neurexin-1β binding to neuroligin-1 triggers the preferential recruitment of PSD-95 versus gephyrin through tyrosine phosphorylation of neuroligin-1. Cell reports. 2013; 3:1996–2007. doi:10.1016/j.celrep.2013.05.013. [PubMed: 23770246]

41. Engert F, Bonhoeffer T. Dendritic spine changes associated with hippocampal long-term synaptic plasticity. Nature. 1999 doi:10.1038/19978.

42. Bosch M, et al. Structural and molecular remodeling of dendritic spine substructures during long-term potentiation. Neuron. 2014; 82:444–459. doi:10.1016/j.neuron.2014.03.021. [PubMed: 24742465]

43. Meyer D, Bonhoeffer T, Scheuss V. Balance and stability of synaptic structures during synaptic plasticity. Neuron. 2014; 82:430–443. doi:10.1016/j.neuron.2014.02.031. [PubMed: 24742464]

44. Kwon H-BB, et al. Neuroligin-1-dependent competition regulates cortical synaptogenesis and synapse number. Nature neuroscience. 2012; 15:1667–1674. doi:10.1038/nn.3256. [PubMed: 23143522]

45. Woods GF, Oh WC, Boudewyn LC, Mikula SK, Zito K. Loss of PSD-95 enrichment is not a prerequisite for spine retraction. The Journal of neuroscience : the official journal of the Society for Neuroscience. 2011; 31:12129–12138. doi:10.1523/JNEUROSCI.6662-10.2011. [PubMed: 21865455]

46. Wu G, Deisseroth K, Tsien R. Spaced stimuli stabilize MAPK pathway activation and its effects on dendritic morphology. Nature neuroscience. 2001; 4:151–158. doi:10.1038/83976. [PubMed: 11175875]

47. Sun Q, Turrigiano GG. PSD-95 and PSD-93 play critical but distinct roles in synaptic scaling up and down. The Journal of neuroscience : the official journal of the Society for Neuroscience. 2011; 31:6800–6808. doi:10.1523/JNEUROSCI.5616-10.2011. [PubMed: 21543610]

48. Makino H, Malinow R. Compartmentalized versus Global Synaptic Plasticity on Dendrites Controlled by Experience. Neuron. 2011; 72:1001–1011. doi:10.1016/j.neuron.2011.09.036. [PubMed: 22196335]

49. Frank CA, Pielage J, Davis GW. A presynaptic homeostatic signaling system composed of the Eph receptor, ephexin, Cdc42, and CaV2.1 calcium channels. Neuron. 2009; 61:556–569. doi:10.1016/ j.neuron.2008.12.028. [PubMed: 19249276]

50. Ebert DH, Greenberg ME. Activity-dependent neuronal signalling and autism spectrum disorder. Nature. 2013; 493:327–337. doi:10.1038/nature11860. [PubMed: 23325215]

51. McClelland A, Sheffler-Collins S, Kayser M, Dalva M. Ephrin-B1 and ephrin-B2 mediate EphB-dependent presynaptic development via syntenin-1. Proceedings of the National Academy of Sciences of the United States of America. 2009; 106:20487–20492. doi:10.1073/pnas.0811862106. [PubMed: 19915143]

52. Yokoyama N, et al. Forward signaling mediated by ephrin-B3 prevents contralateral corticospinal axons from recrossing the spinal cord midline. Neuron. 2001; 29:85–97. [PubMed: 11182083]

53. Leslie K, Nelson S, Turrigiano G. Postsynaptic depolarization scales quantal amplitude in cortical pyramidal neurons. The Journal of neuroscience : the official journal of the Society for Neuroscience. 2001; 21

54. Lois C, Hong E, Pease S, Brown E, Baltimore D. Germline transmission and tissue-specific expression of transgenes delivered by lentiviral vectors. Science (New York, N.Y.). 2002; 295:868–872. doi:10.1126/science.1067081.

55. Takasu M, Dalva M, Zigmond R, Greenberg M. Modulation of NMDA receptor-dependent calcium influx and gene expression through EphB receptors. Science (New York, N.Y.). 2002; 295:491–495. doi:10.1126/science.1065983.
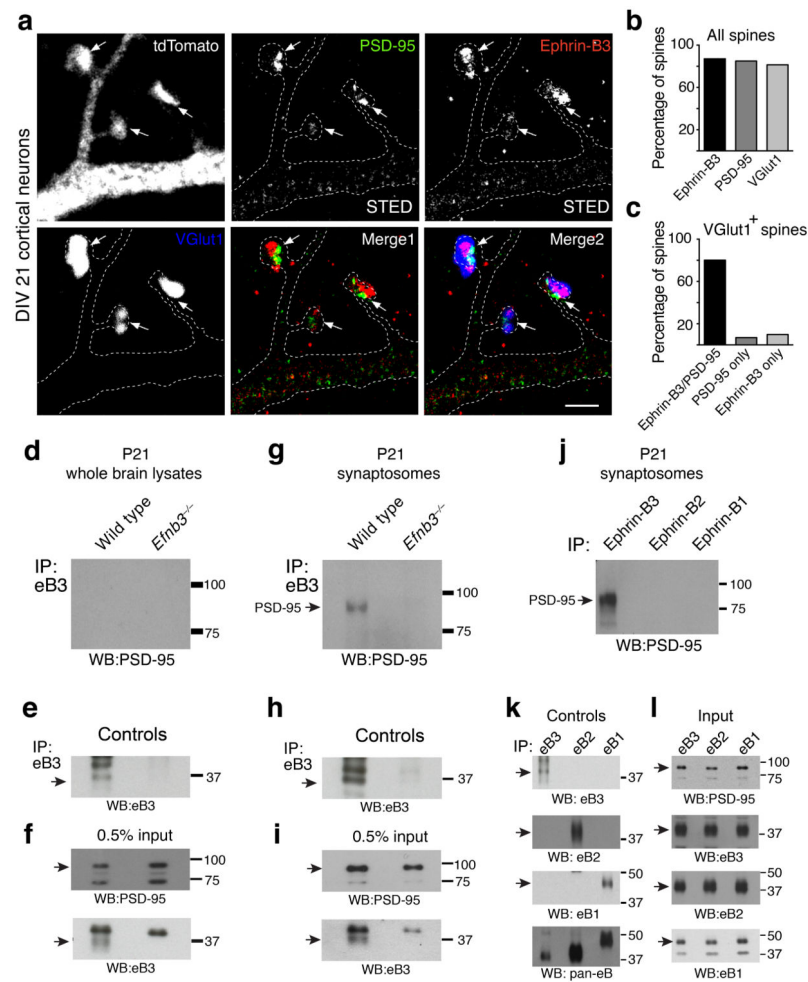
Figure 1. PSD-95 is in a complex with ephrin-B3 at synapses

a) STimulated Emission Depletion (STED) imaging of PSD-95 and ephrin-B3 at synapses. DIV21 tdTomato transfected rat cortical neurons were labeled with the indicated antibodies. PSD-95 and ephrin-B3 were imaged at super-resolution using STED (~80 nm). VGlut1 and tdTomato were imaged at conventional resolution (~250 nm) using confocal. Images are high contrast examples of PSD-95, ephrin-B3 and vGlut1 immunostaining. Arrows indicate PSD-95, ephrin-B3 and vGlut1 co-clusters in dendritic spines. Scale bar: 2 μm. **b)** PSD-95, ephrin-B3 and vGlut1 are found in most (80%) spines (248 spines on 15 neurons, two separate experiments). **c)** PSD-95-ephrin-B3 co-clusters are found predominantly in vGlut[+] spines (162 PSD-95-ephrin-B3 containing spines out of 202 vGlut1[+] spines). Single PSD-95 (14 out of 202 vGlut[+] spines) or ephrin-B3 (20 out of 202 vGlut[+] spines) clusters are rarely found at synapses. **d-f)** Co-immunoprecipitation (co-IP) of ephrin-B3 and PSD-95 from P21 wild type and *Efnb3*^{−/−} mouse whole brain lysates. The efficacy of ephrin-B3 IP **(e)** and input **(f)** are shown for each condition. **(g-i)** PSD-95-ephrin-B3 co-IP from synaptosomes of wild type and *Efnb3*^{−/−} animals **(g).** Control immunoblots indicating the amount of ephrin-B3 IP **(h)** and input **(i)**. **(j)** PSD-95 selectively co-IPs with ephrin-B3 in synaptosomes isolated from P21 wild type brains despite the efficient IP **(k)** and presence **(l)** of each of the

three ephrin-B family members (eB1-3). Representative western blots of three independent experiments from at least three wild type and *Efnb3*$^{-/-}$ animals are shown.
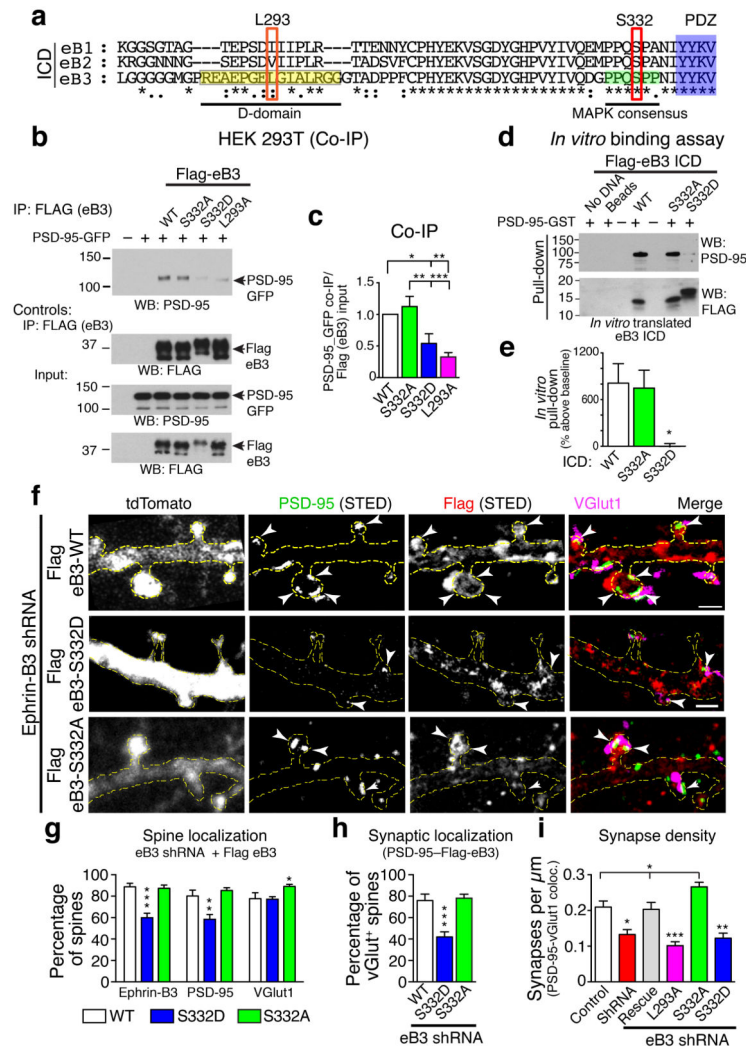
Figure 2. Ephrin-B3 links MAPK signaling to PSD-95-ephrin-B3 interaction and localization
(**a**) Sequence alignment of intracellular domains (ICD) of ephrin-B (eB1-3) family. ERK binding D-Domain in the juxtamembrane region of ephrin-B3 (yellow box) and a putative MAPK phosphorylation motif (green box). Red boxes indicate the positions of point mutations in the D-domain (L293A) and in the putative MAPK phosphorylation motif (S332A/S332D). (**b**) Immunoprecipitation, using antibodies to Flag, of HEK 293T lysates transfected with PSD-95-GFP and indicated flag-tagged ephrin-B3 (flag-eB3) constructs. (**c**) Quantification of co-IP experiments shown in **b** (ANOVA, $F(3, 23) = 9.842$. WT-S332D: p = 0.0475, WT-L293A: p = 0.0034, S332A-S332D: p = 0.0087, S332A-L293A: p = 0.0006; n = 6 blots from separate transfections). (**d**) *In vitro* generated flag-tagged wild type and mutant ephrin-B3 ICDs used to pull down PSD-95-GST. Direct interaction between the two proteins is disrupted by S332D ephrin-B3 ICD. (**e**) Quantification of pull-down experiments from **d** (ANOVA, $F(2, 9) = 2.823$, Fisher's LSD post-hoc, p = 0.0176 (WT-S332D), p = 0.0257 (S332A-S332D); n = 4 independent *in vitro* binding experiments). (**f**) Representative high contrast STED images of DIV21 neurons transfected with tdTomato, ephrin-B3 (eB3) shRNA and indicated flag-eB3 rescue constructs. Arrowheads indicate co-localized, flag-
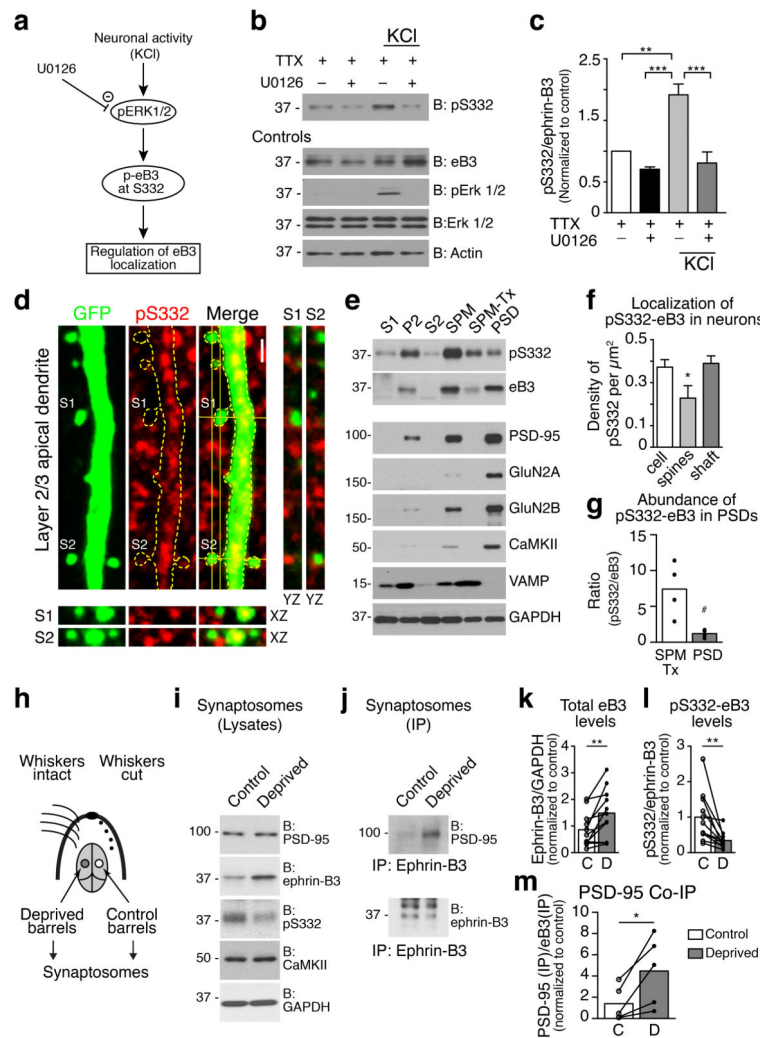
ephrin-B3/PSD-95/vGlut1 clusters. Scale bars**:**, 1 μm. **(g)** Quantification of spine localization of flag-ephrin-B3 (ANOVA, $F_{(2, 88)}$ = 17.58, p = 0.0001), PSD-95 (ANOVA, $F_{(2, 88)}$ = 16.01, p = 0.0029) and vGlut1 (ANOVA, $F_{(2, 88)}$ = 7.536, p = 0.0168), in wild type (n=12 cells, 89 spines), S332D (n=32 cells, 318 spines) and S332A (n=36 cells, 247 spines) transfected neurons. **(h)** Quantification of synaptic PSD-95-ephrin-B3 co-cluster localization in vGlut1[+] dendritic spines in wild type (n=12 cells, 65 vGlut1[+] spines), S332D (n=32 cells, 248 vGlut1[+] spines) and S332A (n=36 cells, 212 vGlut1[+] spines) transfected neurons. ANOVA, $F_{(2, 88)}$ = 20.75, p = 0.0001. **(i)** Quantification of synapse density in DIV14 neurons transfected with ephrin-B3 shRNA and indicated ephrin-B3 rescue constructs by measuring the co-localization of PSD-95 and vGlut1 in conventional confocal mode (ANOVA, $F_{(5, 204)}$ = 19.81, Fisher's LSD, Control-S332A: p = 0.0103, Control-S332D: p = 0.0003, Control-L293A, p < 0.0001, Control-shRNA: p = 0.0015, shRNA-S332A: p<0.0001, rescue-S332A: p = 0.0015, L293A-S332A and S332A-S332D: p<0.0001; control, n=27 cells; eB3shRNA, n=28 cells; eB3L293A, n=42 cells; eB3-S332A, n=43 cells; eB3-S332D, n=30 cells). Representative image are shown in supplementary figure 1. All data are represented as the mean ± s.e.m. *p<0.05, **p<0.01, ***p<0.001, ANOVA, Tukey's post-hoc, unless otherwise stated.

Figure 3. ERK phosphorylation of S332 regulates subcellular localization of ephrin-B3
(**a**) Schematic representation of the experiments. (**b**) Representative immunoblots of lysates from DIV14 rat cortical neurons treated with TTX (1μM, 4 hr.) and U0126 (10μM, 4 hr.) to block activity and ERK activation, respectively. Depolarization with KCl (55mM, 1 hr.) was used to elevate ERK activity. (**c**) Ratio of pS332 to ephrin-B3 signals was used to quantify the effect of neuronal activity on S332 phosphorylation (ANOVA, F (3, 12) = 19.27, Tukey's post-hoc, TTX-KCl: p = 0.0012, TTX+U0126-KCl: p<0.0001, KCl-KCl+U0126: p = 0.0002; n = 4 independent cultures, **p<0.01, ***p<0.001). (**d**) Apical dendrite of GFP labeled layer 2/3 pyramidal neuron stained with pS332. Scale bar: 3 μm. Orthogonal (YZ/XZ) views of spines (S1 and S2) and dendritic shaft (dotted line) show that pS332 staining is primarily localized to the shaft. (**e**) PSD fractionation of P21-23 wild type cortex. Ephrin-B3 is enriched in the PSD fraction along with PSD-95 and other post-synaptic proteins (GluN2A/B subunits, CaMKII). High pS332 signal is observed in extra-synaptic SPM-Tx and S2 fractions.. (**f**) Quantification of pS332 density per area of a neuron, dendritic spines and dendritic shafts from **d** (ANOVA, F (2, 60) = 4.087, Fisher's LSD, p = 0.0237 (cell//spine), p = 0.0115 (spine//dendrite); n = 21 pyramidal neurons). (**g**)

Quantification of relative pS332 ephrin-B3 abundance at synapses from **e**. ([#]p = 0.0171, un-paired t-test (two-tailed), t=3.266, df=6; n=4 independent brain fractionations). Data are represented as means with individual data points.. **h)** Schematic of the sensory deprivation experiment. **i)** Immonoblots of synaptosomal lysates probed with the indicated antibodies. **j)** Immunoblots of PSD-95-ephrin-B3 co-IP from control and sensory deprived barrel cortex. **k)** Quantification of total ephrin-B3 levels normalized to GAPDH in control and deprived synaptosomes (**p = 0.0058, two-tailed paired t-test; t=3.494, df=10; n = 11 pairs). **l)** Quantification of pS332 levels relative to total ephrin-B3 in control and deprived synaptosomes (**p = 0.0080, two-tailed paired t-test; t=3.303, df=10; n = 11 pairs). **m)** Quantification of the amount of PSD-95 co-IP with ephrin-B3 in control and deprived synaptosomes (*p = 0.0313, two-tailed paired t-test; t=3.255, df=4; n = 5 pairs). Graphs (k-m) show the mean (box) and individual control and deprived synaptosome pairs (dots). Graphs in (c) and (f) show the mean ± s.e.m.
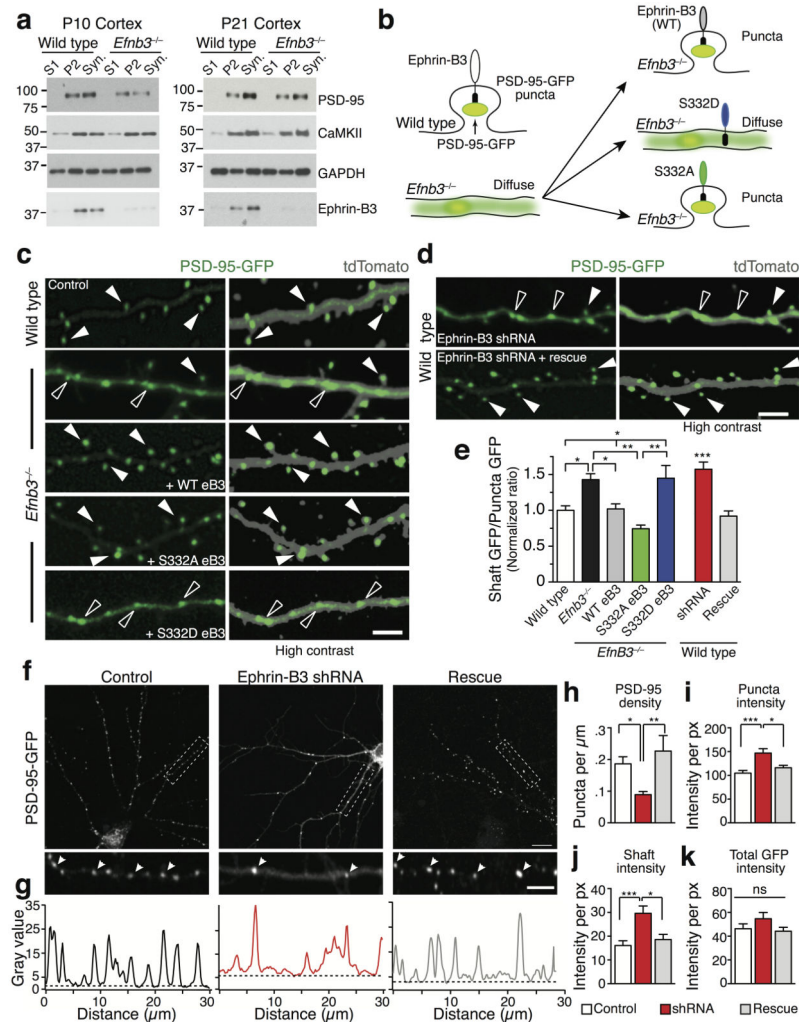
Figure 4. Ephrin-B3 regulates subcellular PSD-95 localization
(a) Western blots of non-synaptic (S1), crude synaptosomal (P2) and pure synaptosomal
(Syn.) fractions from cortices of P10 and P21 wild type and *Efnb3*^{-/-} mice probed with the
indicated antibodies. Less synaptic enrichment of PSD-95 is observed in synaptosomes from
Efnb3^{-/-} mice. (b) Model and predicted outcomes for the organotypic slice culture
experiment. (c-d) Representative two-photon images of cortical pyramidal neurons from
wild type and *Efnb3*^{-/-} organotypic slices transfected with PSD-95-GFP and the indicated
ephrin-B3 rescue constructs. Right panels in **c** and **d** are the high contrast representations of
tdTomato and PSD-95-GFP. Filled arrowheads indicate PSD-95-GFP localized to a spine;
open arrowheads show PSD-95-GFP localized in the dendritic shaft. PSD-95-GFP is
diffusely localized in dendritic shafts of *Efnb3*^{-/-} neurons (c) and ephrin-B3 shRNA-
transfected wild type neurons (d). Scale bar in **c, d**: 5 μm. (e) The ratio of average GFP pixel
intensities in dendritic shafts to the GFP intensities per pixel in puncta was used to measure
the fraction of diffuse PSD-95-GFP in **c-d** (ANOVA, $F_{(4, 93)}$ = 7.155, p-values: wild type//
Efnb3^{-/-}: 0.0105, wild type//*Efnb3*^{-/-} + S332D: 0.0233, *Efnb3*^{-/-}//*Efnb3*^{-/-} + wt-eB3:
0.0285, *Efnb3*^{-/-}//*Efnb3*^{-/-} + S332A: 0.0015, *Efnb3*^{-/-} + wt-eB3//*Efnb3*^{-/-} + S332D:
0.0487, *Efnb3*^{-/-} + S332A//*Efnb3*^{-/-} + S332D: 0.0027; wild type (n = 22), *Efnb3*^{-/-} (n =

31), *Efnb3*$^{-/-}$ + WT eB3 (n = 18), *Efnb3*$^{-/-}$ + S332A (n = 9), *Efnb3*$^{-/-}$ + S332D (n=18) neurons and ANOVA, F (2, 60) = 18.45, wild type//wild type + shRNA (n = 25 neurons): p<0.0001, wild type + shRNA//wild type + shRNA + rescue: p<0.0001 (n = 16 neurons). **(f)** Representative images of DIV10 neurons co-transfected with PSD-95-GFP and either control (pSuper, n = 17 neurons), ephrin-B3 shRNA (n = 17 neurons) or ephrin-B3 shRNA + shRNA ephrin-B3 (rescue, n = 13 neurons) constructs at DIV0. Scale bar: 10 μm. Lower panels show high-resolution images of PSD-95-GFP puncta (arrowheads) from the section of a dendrite shown by the white square in upper panels. Scale bar: 3 μm. **(g)** Plot profiles showing the pattern of PSD-95-GFP localization along the section of dendritic shaft in **f**. Quantification of: **(h)** PSD-95-GFP puncta density, F (2, 44) = 6.322, *p = 0.0365, **p = 0.0043, **(i)** average pixel intensities of GFP fluorescence in puncta; F (2, 44) = 10.16, *p = 0.0127, ***p = 0.0002, **(j)** average pixel intensities of GFP fluorescence in dendritic shafts; F (2, 44) = 8.496, *p=0.0133, ***p=0.0009, and **(k)** Average pixel intensities of total GFP fluorescence (puncta + shaft) per neuron (ANOVA, F (2, 44) = 1.527, p=0.2284) from experiments shown in **f**. Averages were obtained from at least three independent experiments. All data are represented as the mean ± s.e.m. *p<0.05, **p<0.01, ***p<0.001, one way ANOVA with Tukey's post hoc.
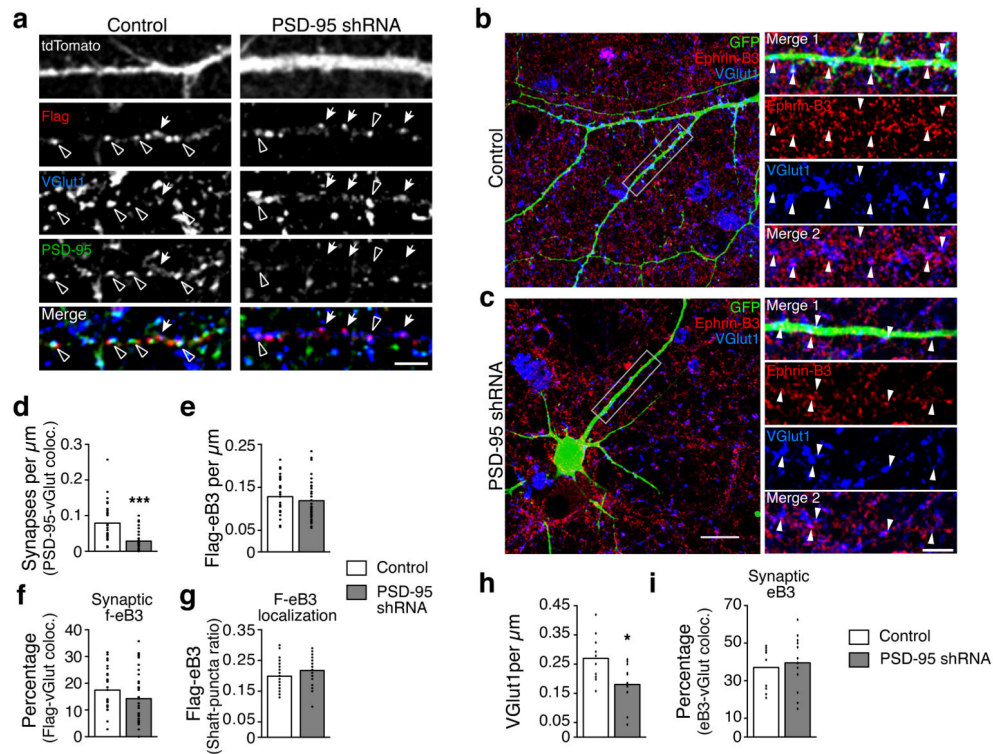
Figure 5. Organization and localization of ephrin-B3 is independent of PSD-95
a) Immunostaining of DIV10 neurons co-transfected with tdTomato, wild type flag-ephrin-B3 and either control (n = 30 neurons) or PSD-95 shRNA (n = 34 neurons) constructs at DIV0. Ephrin-B3 is localized to synapses (arrowheads: vGlut1/PSD-95/Flag, arrows: vGlut1/Flag colocalization) and displays punctate organization in both control and PSD-95 shRNA transfected neurons. **b-c)** Localization of endogenous ephrin-B3 in DIV10 neurons transfected with GFP and either **b)** control (n =10 neurons) or **c)** PSD-95 shRNA (n = 12 neurons) constructs. **d-g)** Quantification of: **d)** synapse density (vGlut1/PSD-95 colocalization, p < 0.0001, t=4.872, df=62); **e)**, Flag-ephrin-B3 puncta density (p = 0.4130, t=0.8241 df=62); **f)** fraction of synaptic ephrin-B3 (vGlut1-Flag colocalization, p = 0.1686, t=1.393, df=62) and **g)** pattern of ephrin-B3 expression (ratio of Flag in shaft/Flag in puncta, p=0.1101, t=1.623, df=57). **h)** Synapse density shown by vGlut1 immunostaining is significantly reduced in PSD-95 shRNA transfected neurons **(c)** compared to control **(b)**, p=0.0114, t=2.785, df=20. **i)** The fraction of synaptic ephrin-B3 (quantified as a percent of ephrin-B3 colocalization with vGlut1, arrowheads in **b** and c) is unchanged between control and PSD-95 shRNA transfected neurons (p=0.6654, t=0.4390, df=20). All data are represented as mean (box) and individual data points (dots). *p<0.05, ***p<0.001, unpaired (two-tailed) t-test.
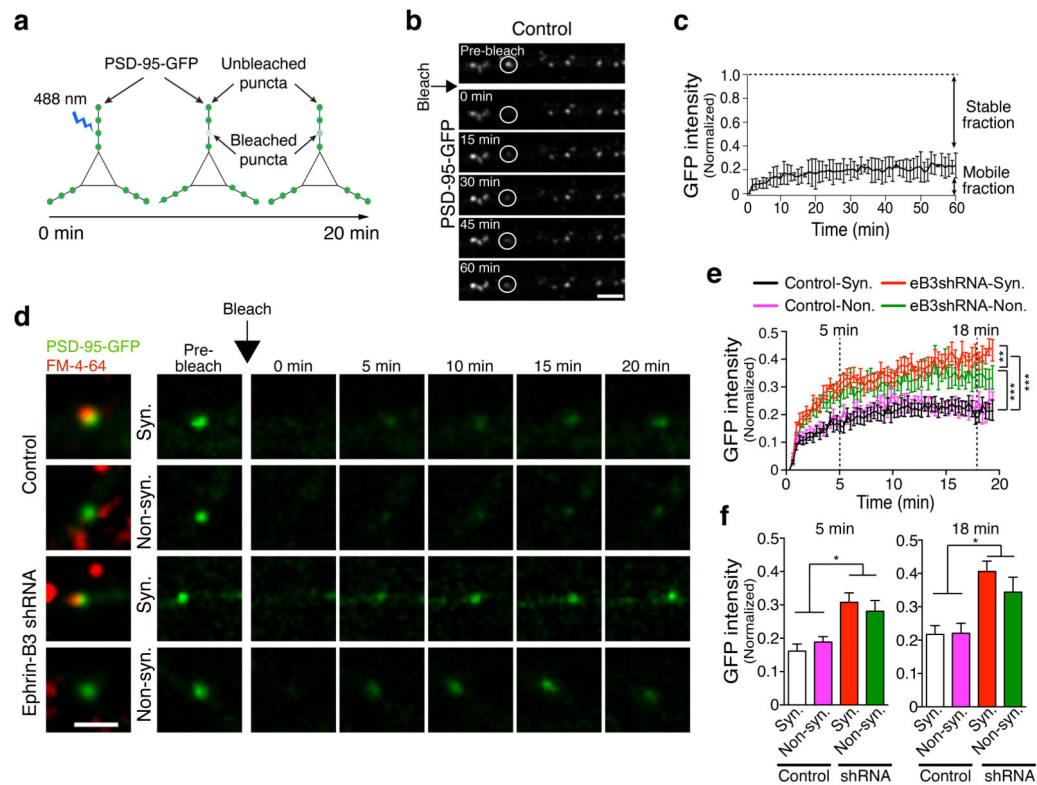
Figure 6. Ephrin-B3 regulates PSD-95 mobility
(a) Schematic of FRAP experiments. **(b)** Representative FRAP images of DIV10 rat cortical neurons transfected with PSD-95-GFP. Recovery of bleached puncta (circle) was monitored for 1 hour with 1-minute intervals. Scale bar: 3μm. **(c)** Recovery plots of 1-hour FRAP experiments (n = 6 neurons, 3 independent experiments). Mean recovery curve ± s.e.m. **(d)** Cortical neurons transfected with PSD-95-GFP and either control or ephrin-B3 shRNA at DIV0. At DIV10 neurons were loaded with FM 4-64 (shown in high contrast) to mark presynaptic release sites. Representative FRAP images of synaptic (Control, n = 25; shRNA, n = 16) and non-synaptic (Control, n = 15; shRNA, n = 11) PSD-95-GFP puncta from at least three independently transfected neurons. Scale bar: 2 μm. **(e)** Quantification of FRAP in (d). Graphs represent mean recovery curve error bars show s.e.m. (Kolmogorov-Smirnov (K-S) test: control-Syn., eB3 shRNA-Syn. ***p<0.0001; control-Non., eB3 shRNA-Non., ***p<0.0001; eB shRNA-Syn., eB3 shRNA-Non., **p = 0.0002). **(f)** Mobile fractions of synaptic (Syn.) and non-synaptic (Non-syn.) PSD-95-GFP puncta at early (5 minutes) and late (18 minutes) phases of FRAP in ephrin-B3 shRNA transfected neurons compared to the control (5 min, $F_{(3, 63)} = 8.860$, Control-Syn.//shRNA syn.: p < 0.0001, Control-Syn.//shRNA Non-syn.: p = 0.0015, Control Non-syn.//shRNA Syn.: p = 0.0015, Control Non-syn//shRNA Non-syn: 0.0228; 18 min, $F_{(3, 63)} = 8.883$, Control-Syn.//shRNA syn.: p <0.0001, Control-Syn.//shRNA Non-syn.: p = 0.0089, Control Non-syn.//shRNA Syn.: p = 0.0002, Control Non-syn.//shRNA Non-syn.: 0.0196. Graphs (f) show the mean ± s.e.m. *p<0.05 one way ANOVA with Fisher's LSD post-hoc.
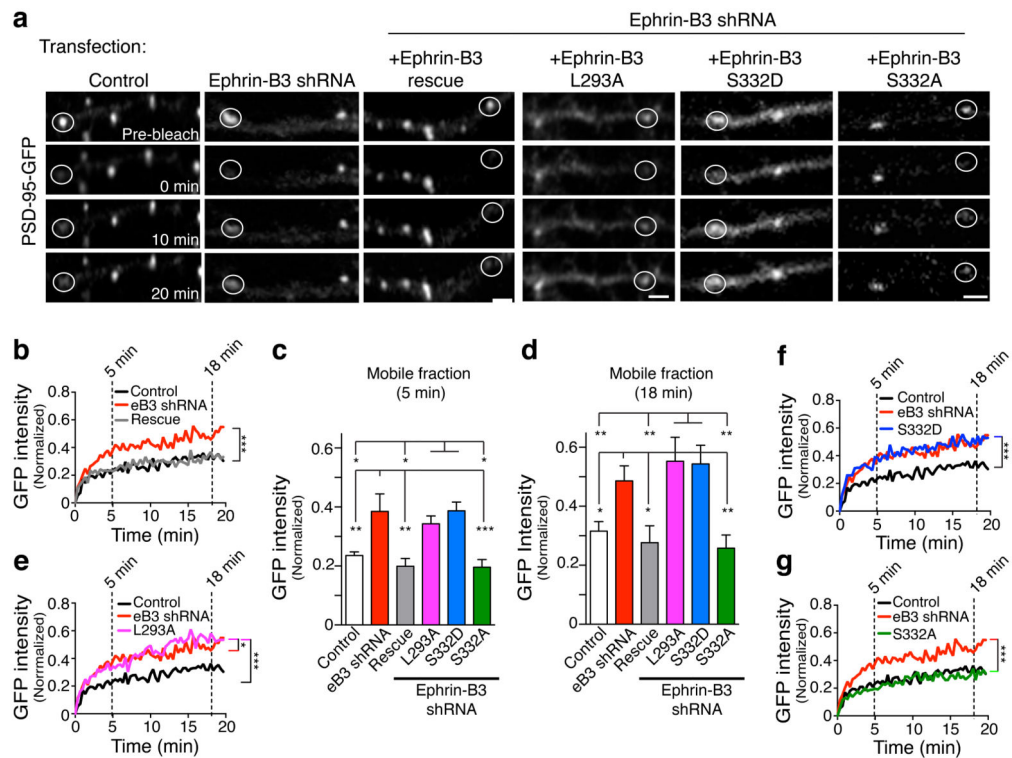
Figure 7. Ephrin-B3 regulation of PSD-95 mobility requires ERK-binding D-domain and S332
(a) Representative FRAP images of DIV10 cortical neurons transfected with PSD-95-GFP, control (pSuper), ephrin-B3 shRNA and indicated ephrin-B3 rescue constructs. Encircled PSD-95-GFP puncta were photobleached. Scale bars: 3μm. **(b, e-g)** Recovery curves of bleached PSD-95-GFP in control (n = 10), ephrin-B3 shRNA (n =12) and **(b)** wild type (n = 9), **(e)** L293A (n = 10), **(f)** S332D (n = 9), **(g)** S332A (n = 8) ephrin-B3 rescue constructs. The recovery of PSD-95-GFP in each rescue condition was plotted separately for clarity (Kolmogorov-Smirnov test, *p<0.05, ***p<0.0001). **(c-d)** PSD-95-GFP mobile fractions at 5 minutes (ANOVA, F (5, 51) = 5.615, p values: Control//shRNA: 0.0043, Control//L293A: 0.0439, Control//S332D: 0.0067, rescue//shRNA: 0.001, shRNA//S332A: 0.0009, rescue// L293A: 0.0122, rescue//S332D: 0.0017, S332A//L293A: 0.0104, S332A//S332D: 0.0014) and 18 minutes (ANOVA, F (5, 51) = 5.385, p values: Control//shRNA: 0.0291, Control// L293A: 0.0043, Control//S332D: 0.0072, rescue//shRNA:0.0126, shRNA//S332A: 0.007, rescue//L293A: 0.0019, rescue//S332D: 0.0032, , S332A//L293A: 0.001, S332A//S332D: 0.0017) of FRAP calculated from the recovery plots in **(b, e-g)**. Data in (f, g) are represented as the mean ± s.e.m. *p<0.05, **p<0.01, ***p<0.001, one way ANOVA with Fisher's LSD post hoc.
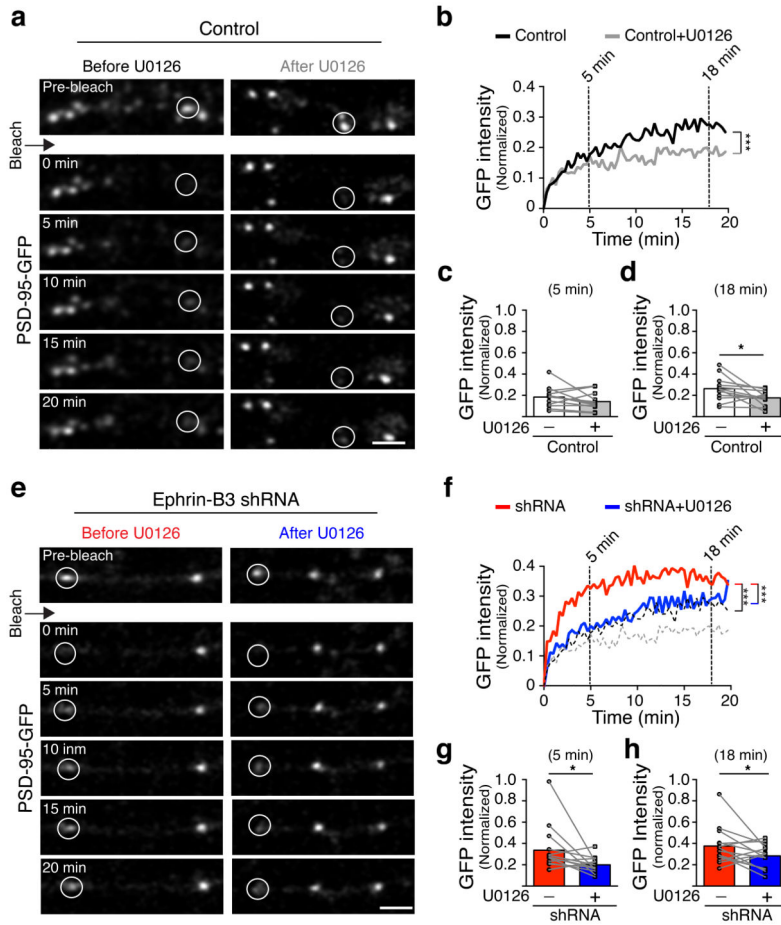
Figure 8. MAPK negatively regulate PSD-95 mobility

(**a**) Representative FRAP images of DIV10 control (n = 12) neurons co-transfected with PSD-95-GFP and pSuper constructs at DIV0 before and after treatment with U0126. Circles indicate PSD-95-GFP puncta that were photobleached. Scale bar, 3 μm. (**b**) Average FRAP traces from control neurons (K-S test, p<0.0001). (**c-d**) PSD-95-GFP mobile fraction in control neurons before and after treatment with U0126 at early (5 min, p = 0.0821; t=1.490, df=11) and late (18 min, p = 0.0203; t=2.319, df=11) phases of FRAP. (**e**) Representative FRAP images of DIV10 neurons transfected with PSD-95-GFP and ephrin-B3 shRNA (n = 14) before and after treatment with U0126**. (f)** Average FRAP traces (K-S test, ***p<0.0001, dotted lines represent control traces from **b**). (**g, h**) PSD-95-GFP mobile fraction in ephrin-B3 shRNA transfected neurons before and after treatment with U0126 at 5 min (p = 0.0216; t=2.240, df=13) and 18 min (p = 0.0329; t=2.009, df=13) of recovery. Data are represented as paired observations (before and after U0126 treatment) of all neurons tested in control and ephrin-B3 shRNA conditions. *p<0.05, two-tailed paired Student's t test.